Available online at www.sciencedirect.com
SCIENCE DIRECT®
International Journal of Plasticity 21 (2005) 397–434
INTERNATIONAL JOURNAL OF Plasticity
www.elsevier.com/locate/ij-

A framework for multiplicative elastoplasticity with kinematic hardening coupled to anisotropic damage

A. Menzel [a,*], M. Ekh [b], K. Runesson [c], P. Steinmann [a]

[a] *Department of Mechanical and Process Engineering, Chair of Applied Mechanics, University of Kaiserslautern, P.O. Box 3049, D-67653 Kaiserslautern, Germany*
[b] *Department of Applied Mechanics, School of Mechanical Engineering, Chalmers University of Technology, SE-412 96 Göteborg, Sweden*
[c] *Department of Structural Mechanics, School of Civil Engineering, Chalmers University of Technology, SE-412 96 Göteborg, Sweden*

Received in final revised form 5 December 2003
Available online 21 February 2004

Abstract

The objective of this contribution is the formulation and algorithmic treatment of a phenomenological framework to capture anisotropic geometrically nonlinear inelasticity. We consider in particular the coupling of viscoplasticity with anisotropic continuum damage whereby both, proportional and kinematic hardening are taken into account. As a main advantage of the proposed formulation standard continuum damage models with respect to a fictitious isotropic configuration can be adopted and conveniently extended to anisotropic continuum damage. The key assumption is based on the introduction of a damage tangent map that acts as an affine pre-deformation. Conceptually speaking, we deal with an Euclidian space with respect to a non-constant metric. The evolution of this field is directly related to the degradation of the material and allows the modeling of specific classes of elastic anisotropy. In analogy to the damage mapping we introduce an internal variable that determines a back-stress tensor via a hyperelastic format and therefore enables the incorporation of plastic

* Corresponding author.
E-mail addresses: amenzel@rhrk.uni-kl.de (A. Menzel), magnus.ekh@me.chalmers.se (M. Ekh), Kenneth.Runesson@sm.chalmers.se (K. Runesson), ps@rhrk.uni-kl.de (P. Steinmann).
URLs: http://mechanik.mv.uni-kl.de, http://www.am.chalmers.se, http://www.sm.chalmers.se, http://mechanik.mv.uni-kl.de.

0749-6419/$ - see front matter
doi:10.1016/j.ijplas.2003.12.006

anisotropy. Several numerical examples underline the applicability of the proposed finite strain framework.

Keywords: Finite elastoplasticity; Kinematic hardening; Anisotropic damage; Anisotropic hyperelasticity; Fictitious configurations; Finite elements

1. Introduction

In the context of computational material modeling it is a desirable feature to develop finite strain formulations and algorithms that provide sufficient freedom to capture phenomenological effects like elastoplasticity, proportional and kinematic hardening, continuum damage, viscosity and finally anisotropy. Several recent monographs reflect the significance of this wide branch in computational mechanics, naming only a few we refer to the works by Rappaz et al. (2003), Lubarda (2002), Haupt (2000), Khan and Huang (1995), Besseling and van der Giessen (1994), Maugin (1992), Lubliner (1990), Lemaitre and Chaboche (1998) and in view of the underlying numerical treatment an outstanding contribution is given by the late Simo (1998). In this work we develop a sound constitutive framework that incorporates all of the previously mentioned phenomenological effects but, nevertheless, neglects any further influences resulting e.g. from a thermal field. Several established concepts are thereby emphasized and joined together:

Hyperelastic formats for appropriate stress fields are applied and the established assumption of a stress-free intermediated configuration, i.e. multiplicative elastoplasticity, is adopted, see e.g. Haupt (2000) and references cited therein. This nowadays standard framework enables us to incorporated commonly used formulations for the elastic behavior and the effect of proportional hardening. For an alternative framework, see e.g. Svendsen (1998) or Bertram (1999, 2003).

Concerning the introduction of kinematic or rather anisotropic hardening one could either directly set up evolution equations for the back-stress tensor or introduce a corresponding internal variable that determines the back-stress via a hyperelastic format, see Ekh and Runesson (2001), Diegele et al. (2000) or Svendsen (1998) and Svendsen et al. (1998) among others. In this work we adopt the latter approach in analogy to the work by Wallin et al. (2003) (without any restriction to elastic isotropy), i.e. an additional fictitious configuration is formally introduced whose underlying tangent map serves as an internal variable. It is then straightforward to follow the lines of multiplicative elastoplasticity such that an evolution equation for the corresponding kinematic hardening velocity gradient is a natural outcome.

Before coupling the plasticity framework to continuum damage mechanics we have to develop a sound and physical formulation of degradation that provides sufficient freedom to capture the anisotropic nature of damage. Thus the state of damage has to be described by at least a second order tensor, see Leckie and Onat (1981). In this contribution, the underlying mechanism to incorporate the effects of damage is provided by the hypothesis of strain energy equivalence between the

intermediate configuration of multiplicative elastoplasticity and an additional fictitious or rather effective configuration, see Betten (1981), Sidoroff (1981), Murakami (1988), Kattan and Voyiadjis (1990), Oller et al. (1995), Brünig (2003), Steinmann and Carol (1998), Menzel and Steinmann (2001b) and references cited therein. The approach allows the interpretation as covariance of the free energy with respect to superposed isomorphism, which are identified here as the damage deformation gradient, compare Marsden and Hughes (1994), Lu and Papadopoulos (2000), Lu (2003) or Menzel and Steinmann (2003b,c). As an interesting aspect, the present damage metric based formulation may formally be related to the classical understanding of damage as an area reduction since the damage tangent map determines the metric with respect to the intermediate configuration. Apparently, it turns out that this approach includes besides the trivial case of isotropy for spherical damage mappings specific elastic symmetry classes, namely subclasses of transversal isotropy and orthotropy which are of cardinal interest for engineering applications, compare Menzel and Steinmann (2001a). Similar to the plastic part of the deformation gradient and the kinematic hardening mapping the setup of a Lemaitre-type evolution equation for the damage velocity gradient is straightforward.

Based on this, the coupling of the plasticity framework to continuum damage is performed by adopting the concept of effective stress or rather strain equivalence, for a survey see e.g. Lämmer and Tsakmakis (2000), Steinmann et al. (1994) or Lemaitre and Chaboche (1998). In this work, effective stresses are incorporated via modified Mandel-type tensors. Conceptually speaking, the appropriate metric is varied such that anisotropic degradation enters the corresponding stress fields with respect to the intermediate configuration. This approach enables us to describe besides proportional and kinematic hardening effects, as usually observed in metal plasticity, typical path- or rather history-dependent degradation of the material. Initially damaged configurations are conveniently introduced via initial damage metrics that differs from the, say, identity and thereby result in an initially anisotropic elastic response. By applying a spectral decomposition to the initial damage metric, it is obvious that eigenvalues smaller than one then denote degradation and eigenvalues greater than one characterize stiffening compared to a standard isotropic elastic setting where the metric boils down to the identity within an Euclidian setting. The product of these eigenvalues (if smaller than one) allows interpretation as being directly related to the initial content of isotropic damage or rather spherical voids. A distinction between different material behavior in tension and compression, as e.g. the microcrack-opening-closure effect which is addressed in Ekh and Runesson (2000) and Ekh et al. (2003b), is for conceptual clarity not explicitly considered in the elastic response but allows to be shifted to a specific damage evolution law. In this context, the developed framework is not restricted to e.g. anisotropic failure of initially isotropic metals but additionally provides a convenient formulation for the modeling of the material behavior and failure of e.g. fiber reinforced composites and plastics. Furthermore, even constitutive models on the meso or micro level are captured in the presented formulation as successfully developed in Ekh et al. (2003a) where special emphasis is placed on the modeling of single- and polycrystal-(visco)plasticity. Applications of the presented framework within small strain kinematics are given in Menzel et al.

(2002) and Ekh et al. (2003b) while the finite strain formulation is developed in Menzel and Steinmann (2003a).

Concerning the specific model that finally serves for several numerical examples which conclude this contribution, we adopt constitutive equations as simple as possible, i.e. a St. Venant Kirchhoff-type ansatz and a v. Mises-type yield function; for an outline on anisotropic yield functions we refer the reader to, e.g., the contributions by Steinmann et al. (1996), Miehe (1998), Hill (2000), and Bruhns et al. (2003). While the underlying plastic evolution equation as well as the flow of proportional hardening contribution is associated and a plastic spin will be neglected, the kinematic hardening contribution is enhanced by an additional non-associated saturation-type term. However, the non-associated damage model itself is anisotropic and allows to account for different material behavior in tension and compression with respect to the space of the driving damage force. We apply in particular a Rankine-type model as advocated by Carol et al. (2001) and further elaborated in Menzel et al. (2003). This ansatz closes the physically sound framework. Apparently, any appropriate isotropic or anisotropic damage model, which is based on an internal variable of e.g. zero or second order and allows representation via strain energy equivalence, can conveniently be incorporated into the developed framework since the introduced effective space is assumed to be isotropic. Finally, the commonly applied exponential integration scheme is applied to the evolution equation of the plastic, kinematic hardening and the damage velocity gradient. Nevertheless, solely the evolution of the damage contribution with respect to the effective configuration allows representation within the standard spectral decomposition theorem for symmetric second order tensors. Moreover, it turns out that the underlying Jacobians to solve the systems of nonlinear equations as based on Newton-type algorithms are conveniently approximated by a first order difference scheme.

The paper is organized as follows: To set the stage, the underlying kinematics due to the introduction of fictitious configurations are given in Section 2. In order to obtain hyperelastic stress formats, we consequently apply the Coleman–Noll entropy principle within the framework of non-standard dissipative materials, Section 3. Additional emphasis is thereby placed on appropriate evolution equations and essential numerical aspects. A detailed outline of the application of the fictitious configuration concept is highlighted in Section 4 such that later on, in Section 5, a convenient prototype model can be introduced. Finally, several numerical examples underline the applicability of the proposed framework, Section 6, and a brief summary in Section 7 concludes the paper.

2. Kinematics

The subsequent section summarizes some essentials of the kinematic setup in nonlinear continuum mechanics. Special emphasis is placed on the introduction of the considered additional fictitious configurations and the underlying tangent maps.

For a detailed outline we refer the reader to the monographs by Haupt (2000), Marsden and Hughes (1994), Lodge (1974) or Eringen (1962).

Let the reference configuration of the body B of interest be denoted by $\mathscr{B}_0$. The nonlinear motion is defined by the mapping $\boldsymbol{\varphi}(\boldsymbol{X},t) : \mathscr{B}_0 \times \mathbb{R} \rightarrow \mathscr{B}_t$ which transforms position vectors of material points $\boldsymbol{X}$ in $\mathscr{B}_0$ to spatial position vectors $\boldsymbol{x} = \boldsymbol{\varphi}(\boldsymbol{X},t)$ in $\mathscr{B}_t$ whereby t characterizes the time. Local natural tangent spaces as well as their dual spaces are denoted by $T\mathscr{B}_0$, $T^*\mathscr{B}_0$ and $T\mathscr{B}_t$, $T^*\mathscr{B}_t$, respectively, which enables us to introduce the underlying metric tensors, identities and linear tangent maps as

$$\begin{aligned} &\boldsymbol{G} : T\mathscr{B}_0 \rightarrow T^*\mathscr{B}_0, \quad \boldsymbol{G}^{-1} : T^*\mathscr{B}_0 \rightarrow T\mathscr{B}_0, \quad \boldsymbol{I} : T\mathscr{B}_0 \rightarrow T\mathscr{B}_0, \quad \boldsymbol{F} : T\mathscr{B}_0 \rightarrow T\mathscr{B}_t, \\ &\boldsymbol{g} : T\mathscr{B}_t \rightarrow T^*\mathscr{B}_t, \quad \boldsymbol{g}^{-1} : T^*\mathscr{B}_t \rightarrow T\mathscr{B}_t, \quad \boldsymbol{i} : T\mathscr{B}_t \rightarrow T\mathscr{B}_t, \quad \boldsymbol{f} : T\mathscr{B}_t \rightarrow T\mathscr{B}_0 \end{aligned} \tag{1}$$

with $\boldsymbol{I} = \boldsymbol{f} \cdot \boldsymbol{F}$, $\boldsymbol{i} = \boldsymbol{F} \cdot \boldsymbol{f}$ and $\det(\boldsymbol{F}), \det(\boldsymbol{f}) > 0$, compare Fig. 1. Based on this, several kinematic tensors can be introduced, e.g.

$$\begin{aligned} &\boldsymbol{B} = \boldsymbol{\varphi}^* \boldsymbol{g}^{-1} = \boldsymbol{f} \star \boldsymbol{g}^{-1} = \boldsymbol{f} \cdot \boldsymbol{g}^{-1} \cdot \boldsymbol{f}^{\mathrm{d}}, \quad \boldsymbol{C} = \boldsymbol{\varphi}^* \boldsymbol{g} = \boldsymbol{f} \star \boldsymbol{g} = \boldsymbol{F}^{\mathrm{d}} \cdot \boldsymbol{g} \cdot \boldsymbol{F}, \\ &\boldsymbol{b} = \boldsymbol{\varphi}_* \boldsymbol{G}^{-1} = \boldsymbol{F} \star \boldsymbol{G}^{-1} = \boldsymbol{F} \cdot \boldsymbol{G}^{-1} \cdot \boldsymbol{F}^{\mathrm{d}}, \quad \boldsymbol{c} = \boldsymbol{\varphi}_* \boldsymbol{G} = \boldsymbol{F} \star \boldsymbol{G} = \boldsymbol{f}^{\mathrm{d}} \cdot \boldsymbol{G} \cdot \boldsymbol{f}, \end{aligned} \tag{2}$$

whereby the notation $[\bullet]^{\mathrm{d}}$ abbreviates the dual of a (second order) field; to give an example $\boldsymbol{v} \cdot \boldsymbol{F} = \boldsymbol{F}^{\mathrm{d}} \cdot \boldsymbol{v} \; \forall \; \boldsymbol{v} : T\mathscr{B}_t \rightarrow \mathbb{R}$ with $\boldsymbol{F}^{\mathrm{d}} : T^*\mathscr{B}_t \rightarrow T^*\mathscr{B}_0$ being obvious. The setup of generalized strain measures in terms of principal stretches is now

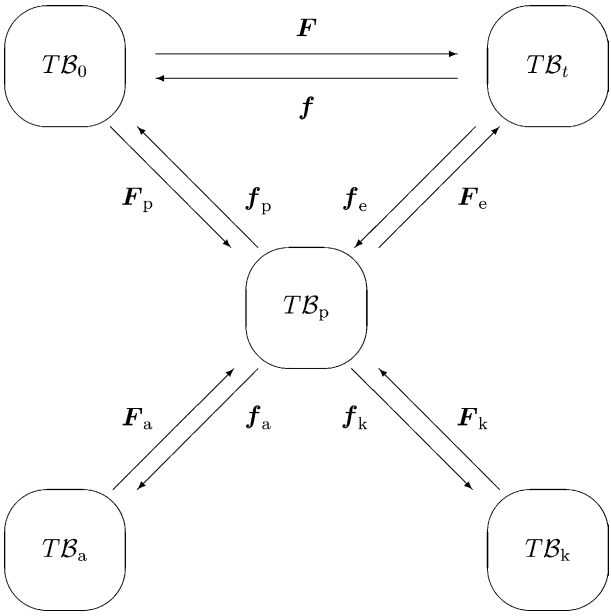

Fig. 1. Graphical representation of the tangent spaces and the linear tangent maps.

straightforward. Nevertheless, we solely consider Green–Lagrange-type tensors in the progression of this work, i.e. $\boldsymbol{E} \doteq \frac{1}{2}[\boldsymbol{C} - \boldsymbol{G}]$.

Adopting the framework of multiplicative elastoplasticty, let the natural and dual tangent space of the underlying intermediate configuration be denoted by $T\mathscr{B}_{\mathrm{p}}$ and $T^*\mathscr{B}_{\mathrm{p}}$, respectively. Similar to Eq. (1), the metric fields, the identity and the corresponding linear tangent maps as based on the multiplicative decomposition ($\boldsymbol{F} \doteq \boldsymbol{F}_{\mathrm{e}} \cdot \boldsymbol{F}_{\mathrm{p}}, \boldsymbol{f} \doteq \boldsymbol{f}_{\mathrm{p}} \cdot \boldsymbol{f}_{\mathrm{e}}$) read

$$\begin{aligned} &\widehat{\boldsymbol{G}} : T\mathscr{B}_{\mathrm{p}} \to T^*\mathscr{B}_{\mathrm{p}}, \quad \widehat{\boldsymbol{G}}^{-1} : T^*\mathscr{B}_{\mathrm{p}} \to T\mathscr{B}_{\mathrm{p}}, \quad \widehat{\boldsymbol{I}} : T\mathscr{B}_{\mathrm{p}} \to T\mathscr{B}_{\mathrm{p}}, \\ &\boldsymbol{F}_{\mathrm{p}} : T\mathscr{B}_0 \to T\mathscr{B}_{\mathrm{p}}, \quad \boldsymbol{f}_{\mathrm{p}} : T\mathscr{B}_{\mathrm{p}} \to T\mathscr{B}_0, \quad \boldsymbol{F}_{\mathrm{e}} : T\mathscr{B}_{\mathrm{p}} \to T\mathscr{B}_t, \quad \boldsymbol{f}_{\mathrm{e}} : T\mathscr{B}_t \to T\mathscr{B}_{\mathrm{p}} \end{aligned} \tag{3}$$

with $\boldsymbol{I} = \boldsymbol{f}_{\mathrm{p}} \cdot \boldsymbol{F}_{\mathrm{p}}$, $\widehat{\boldsymbol{I}} = \boldsymbol{F}_{\mathrm{p}} \cdot \boldsymbol{f}_{\mathrm{p}} = \boldsymbol{f}_{\mathrm{e}} \cdot \boldsymbol{F}_{\mathrm{e}}$, $\boldsymbol{i} = \boldsymbol{F}_{\mathrm{e}} \cdot \boldsymbol{f}_{\mathrm{e}}$ and $\det(\boldsymbol{F}_{\mathrm{p}}), \det(\boldsymbol{f}_{\mathrm{p}}), \det(\boldsymbol{F}_{\mathrm{e}}), \det(\boldsymbol{f}_{\mathrm{e}}) > 0$. Once more, typical kinematic tensors can be constructed in analogy to Eq. (2). Referring to the elastic linear tangent map we define

$$\begin{aligned} &\widehat{\boldsymbol{B}}_{\mathrm{e}} = \boldsymbol{f}_{\mathrm{e}} \bigstar \boldsymbol{g}^{-1} = \boldsymbol{f}_{\mathrm{e}} \cdot \boldsymbol{g}^{-1} \cdot \boldsymbol{f}_{\mathrm{e}}^{\mathrm{d}}, \quad \widehat{\boldsymbol{C}}_{\mathrm{e}} = \boldsymbol{f}_{\mathrm{e}} \bigstar \boldsymbol{g} = \boldsymbol{F}_{\mathrm{e}}^{\mathrm{d}} \cdot \boldsymbol{g} \cdot \boldsymbol{F}_{\mathrm{e}}, \\ &\boldsymbol{b}_{\mathrm{e}} = \boldsymbol{F}_{\mathrm{e}} \bigstar \widehat{\boldsymbol{G}}^{-1} = \boldsymbol{F}_{\mathrm{e}} \cdot \widehat{\boldsymbol{G}}^{-1} \cdot \boldsymbol{F}_{\mathrm{e}}^{\mathrm{d}}, \quad \boldsymbol{c}_{\mathrm{e}} = \boldsymbol{F}_{\mathrm{e}} \bigstar \widehat{\boldsymbol{G}} = \boldsymbol{f}_{\mathrm{e}}^{\mathrm{d}} \cdot \widehat{\boldsymbol{G}} \cdot \boldsymbol{f}_{\mathrm{e}} \end{aligned} \tag{4}$$

and the corresponding elastic Green–Lagrange strain measure consequently reads $\widehat{\boldsymbol{E}}_{\mathrm{e}} \doteq \frac{1}{2}[\widehat{\boldsymbol{C}}_{\mathrm{e}} - \widehat{\boldsymbol{G}}]$. Similar kinematic transformations in terms of $\boldsymbol{F}_{\mathrm{p}}$ follow straightforward and are therefore omitted here.

Finally, on top of the spatial, intermediate and reference configuration, we introduce two additional fictitious configurations – both being attached to the intermediate configuration, see Fig. 1. On the one hand, a fictitious or rather effective configuration is assumed to be isotropic (with respect to e.g. the later introduced free Helmholtz energy density) and the corresponding tangent space and the dual space are denoted by $T\mathscr{B}_{\mathrm{a}}$ and $T^*\mathscr{B}_{\mathrm{a}}$, respectively. The underlying metric fields, the identity and the fictitious linear tangent map read in analogy to Eqs. (1) and (3) as

$$\begin{aligned} &\bar{\boldsymbol{G}} : T\mathscr{B}_{\mathrm{a}} \to T^*\mathscr{B}_{\mathrm{a}}, \quad \bar{\boldsymbol{G}}^{-1} : T^*\mathscr{B}_{\mathrm{a}} \to T\mathscr{B}_{\mathrm{a}}, \quad \bar{\boldsymbol{I}} : T\mathscr{B}_{\mathrm{a}} \to T\mathscr{B}_{\mathrm{a}}, \\ &\boldsymbol{F}_{\mathrm{a}} : T\mathscr{B}_{\mathrm{a}} \to T\mathscr{B}_{\mathrm{p}}, \quad \boldsymbol{f}_{\mathrm{a}} : T\mathscr{B}_{\mathrm{p}} \to T\mathscr{B}_{\mathrm{a}} \end{aligned} \tag{5}$$

with $\bar{\boldsymbol{I}} = \boldsymbol{f}_{\mathrm{a}} \cdot \boldsymbol{F}_{\mathrm{a}}$, $\widehat{\boldsymbol{I}} = \boldsymbol{F}_{\mathrm{a}} \cdot \boldsymbol{f}_{\mathrm{a}}$ and $\det(\boldsymbol{F}_{\mathrm{a}}), \det(\boldsymbol{f}_{\mathrm{a}}) > 0$. These linear tangent maps allow interpretation as an affine pre-deformation and determine the elastic anisotropy of the considered body B as well as the degradation of the material. In analogy to Eqs. (2) and (4), one could introduce several kinematic tensor fields with respect to $\boldsymbol{F}_{\mathrm{a}}$. In the sequel however, we are mainly interested in the pushforward of $\bar{\boldsymbol{G}}^{-1}$ and the pullback of $\widehat{\boldsymbol{E}}_{\mathrm{e}}$, i.e.

$$\widehat{\boldsymbol{A}}^{-1} \doteq \boldsymbol{F}_{\mathrm{a}} \bigstar \bar{\boldsymbol{G}}^{-1} = \boldsymbol{F}_{\mathrm{a}} \cdot \bar{\boldsymbol{G}}^{-1} \cdot \boldsymbol{F}_{\mathrm{a}}^{\mathrm{d}}, \quad \bar{\boldsymbol{E}}_{\mathrm{e}} \doteq \boldsymbol{f}_{\mathrm{a}} \bigstar \widehat{\boldsymbol{E}}_{\mathrm{e}} = \boldsymbol{F}_{\mathrm{a}}^{\mathrm{d}} \cdot \widehat{\boldsymbol{E}}_{\mathrm{e}} \cdot \boldsymbol{F}_{\mathrm{a}}. \tag{6}$$

On the other hand, the natural and dual tangent space of the second fictitious configuration is introduced as $T\mathscr{B}_{\mathrm{k}}$ and $T^*\mathscr{B}_{\mathrm{k}}$, respectively, such that the correlated metric fields, the identity and the linear tangent maps consequently result in

$$\begin{aligned} &\widetilde{\boldsymbol{G}} : T\mathscr{B}_{\mathrm{k}} \to T^*\mathscr{B}_{\mathrm{k}}, \quad \widetilde{\boldsymbol{G}}^{-1} : T^*\mathscr{B}_{\mathrm{k}} \to T\mathscr{B}_{\mathrm{k}}, \quad \widetilde{\boldsymbol{I}} : T\mathscr{B}_{\mathrm{k}} \to T\mathscr{B}_{\mathrm{k}}, \\ &\boldsymbol{F}_{\mathrm{k}} : T\mathscr{B}_{\mathrm{k}} \to T\mathscr{B}_{\mathrm{p}}, \quad \boldsymbol{f}_{\mathrm{k}} : T\mathscr{B}_{\mathrm{p}} \to T\mathscr{B}_{\mathrm{k}} \end{aligned} \tag{7}$$

with $\widetilde{I} = \boldsymbol{f}_{\mathrm{k}} \cdot \boldsymbol{F}_{\mathrm{k}}$, $\widehat{\boldsymbol{I}} = \boldsymbol{F}_{\mathrm{k}} \cdot \boldsymbol{f}_{\mathrm{k}}$ and $(\det(\boldsymbol{F}_{\mathrm{k}}),\ \det(\boldsymbol{f}_{\mathrm{k}}) > 0$. Apparently, the underlying linear mappings serve as internal variables which allow to set up a convenient framework for kinematic hardening. Placing emphasis on corresponding kinematic fields, we are mainly interested in pushforward operations of $\widetilde{\boldsymbol{G}}$, namely

$$\widehat{\boldsymbol{K}} \doteq \boldsymbol{F}_{\mathrm{k}} \bigstar \widetilde{\boldsymbol{G}} = \boldsymbol{f}_{\mathrm{k}}^{\mathrm{d}} \cdot \widetilde{\boldsymbol{G}} \cdot \boldsymbol{f}_{\mathrm{k}} \tag{8}$$

which enables us to set up a strain field of Green–Lagrange-type

$$\widehat{\boldsymbol{E}}_{\mathrm{k}} \doteq \frac{1}{2}[\widehat{\boldsymbol{K}} - \widehat{\boldsymbol{G}}], \quad \bar{\boldsymbol{E}}_{\mathrm{k}} = \boldsymbol{f}_{\mathrm{a}} \bigstar \widehat{\boldsymbol{E}}_{\mathrm{k}} = \boldsymbol{F}_{\mathrm{a}}^{\mathrm{d}} \cdot \widehat{\boldsymbol{E}}_{\mathrm{k}} \cdot \boldsymbol{F}_{\mathrm{a}}. \tag{9}$$

Now, after discussing the transformation relations between different configurations, we place emphasis on the correlated velocity gradients. In this context, let the physical velocity gradient and its pullback to the reference configuration be denoted by

$$\boldsymbol{l} = \mathrm{D}_t \boldsymbol{F} \cdot \boldsymbol{f} = -\boldsymbol{F} \cdot \mathrm{D}_t \boldsymbol{f}\ , \quad \boldsymbol{L} = \boldsymbol{\varphi}^* \boldsymbol{l} = \boldsymbol{f} \bigstar \boldsymbol{l} = \boldsymbol{f}\ \cdot \mathrm{D}_t \boldsymbol{F} = -\mathrm{D}_t \boldsymbol{f}\ \cdot \boldsymbol{F}, \tag{10}$$

whereby the notation D_t abbreviates the material time derivative. A pullback operation with respect to the intermediate configuration results in

$$\widehat{\boldsymbol{L}} = \boldsymbol{f}_{\mathrm{e}} \bigstar \boldsymbol{l} = \boldsymbol{f}_{\mathrm{e}} \cdot \mathrm{D}_t \boldsymbol{F} \cdot \boldsymbol{f}_{\mathrm{p}} = -\boldsymbol{F}_{\mathrm{p}} \cdot \mathrm{D}_t \boldsymbol{f}\ \cdot \boldsymbol{F}_{\mathrm{e}} \tag{11}$$

and referring to the adopted multiplicative decomposition we obtain the following additive decomposition

$$\widehat{\boldsymbol{L}} = \widehat{\boldsymbol{L}}_{\mathrm{e}} + \widehat{\boldsymbol{L}}_{\mathrm{p}} = \boldsymbol{f}_{\mathrm{e}} \cdot \mathrm{D}_t \boldsymbol{F}_{\mathrm{e}} + \mathrm{D}_t \boldsymbol{F}_{\mathrm{p}} \cdot \boldsymbol{f}_{\mathrm{p}} = -\mathrm{D}_t \boldsymbol{f}_{\mathrm{e}} \cdot \boldsymbol{F}_{\mathrm{e}} - \boldsymbol{F}_{\mathrm{p}} \cdot \mathrm{D}_t \boldsymbol{f}_{\mathrm{p}}. \tag{12}$$

A similar outline in, e.g., $\mathscr{B}_0$ or $\mathscr{B}_t$ follows straightforward and is hence omitted here. In analogy to these well-established formats, the velocity gradients with respect to the, say, damage and hardening mapping $\boldsymbol{F}_{\mathrm{a}}$ and $\boldsymbol{F}_{\mathrm{k}}$ are consequently introduced (similar to $\widehat{\boldsymbol{L}}_{\mathrm{p}}$) as

$$\widehat{\boldsymbol{L}}_{\mathrm{a}} \doteq \mathrm{D}_t \boldsymbol{F}_{\mathrm{a}} \cdot \boldsymbol{f}_{\mathrm{a}} = -\boldsymbol{F}_{\mathrm{a}} \cdot \mathrm{D}_t \boldsymbol{f}_{\mathrm{a}}, \quad \widehat{\boldsymbol{L}}_{\mathrm{k}} \doteq \mathrm{D}_t \boldsymbol{F}_{\mathrm{k}} \cdot \boldsymbol{f}_{\mathrm{k}} = -\boldsymbol{F}_{\mathrm{k}} \cdot \mathrm{D}_t \boldsymbol{f}_{\mathrm{k}}. \tag{13}$$

3. Coleman–Noll entropy principle

In this section, we reiterate the application of the Coleman-Noll entropy principle to the problem at hand. For a general overview of the underlying theory we refer the reader to the recent monographs by Lubarda (2002), Haupt (2000), Maugin (1999) and Antman (1995) the work by Miehe and Stein (1992) or Menzel and Steinmann (2003a) and Ekh et al. (2003b).

Let the free Helmholtz energy density take the following format:

$$\psi(\boldsymbol{F}_{\mathrm{e}}, \boldsymbol{F}_{\mathrm{k}}, \boldsymbol{F}_{\mathrm{a}}, \kappa; \boldsymbol{X}) \doteq \psi_{\mathrm{e}}(\widehat{\boldsymbol{E}}_{\mathrm{e}}, \widehat{\boldsymbol{A}}^{-1}; \boldsymbol{X}) + \psi_{\mathrm{k}}(\widehat{\boldsymbol{E}}_{\mathrm{k}}, \widehat{\boldsymbol{A}}^{-1}; \boldsymbol{X}) + \psi_{\kappa}(\kappa; \boldsymbol{X}), \tag{14}$$

whereby a representation with respect to the intermediated setting has been chosen and, as outlined in the previous section, $\widehat{\boldsymbol{E}}_{\mathrm{e}}$, $\widehat{\boldsymbol{E}}_{\mathrm{k}}$, $\widehat{\boldsymbol{A}}^{-1}$ represent the elastic Green–Lagrange strain measure, the Green–Lagrange-type strain measure as based on the

internal kinematic hardening variable as well as the damage metric, respectively, and κ defines an additional scalar-valued (internal) variable that accounts for proportional hardening. The local form of the isothermal Clausius–Duhem inequality consequently reads

$$\begin{aligned}\mathscr{D} = \widehat{\boldsymbol{M}}^{\mathrm{d}}_{\mathrm{e}} : \widehat{\boldsymbol{L}} - \partial_{\widehat{\boldsymbol{E}}_{\mathrm{e}}}\psi : \mathrm{D}_t\widehat{\boldsymbol{E}}_{\mathrm{e}} - \partial_{\widehat{\boldsymbol{E}}_{\mathrm{k}}}\psi : \mathrm{D}_t\widehat{\boldsymbol{E}}_{\mathrm{k}} \\ - \partial_{\widehat{\boldsymbol{A}}^{-1}}\psi : \mathrm{D}_t\widehat{\boldsymbol{A}}^{-1} - \partial_{\kappa}\psi\, \mathrm{D}_t\kappa \geqslant 0\end{aligned} \tag{15}$$

with $\widehat{\boldsymbol{M}}^{\mathrm{d}}_{\mathrm{e}}$ characterizing the Mandel stress which enters the computation of the stress power $\widehat{\boldsymbol{M}}^{\mathrm{d}}_{\mathrm{e}} : \widehat{\boldsymbol{L}}$. Based on the previously highlighted kinematical relations as outlined in Eqs. (4), (6), (8), (12) and (13) we observe the following connections between the (tensorial) material time derivatives (which are incorporated in the dissipation inequality (15)) and the underlying velocity gradients

$$\mathrm{D}_t\widehat{\boldsymbol{E}}_{\mathrm{e}} = [\widehat{\boldsymbol{C}}_{\mathrm{e}} \cdot \widehat{\boldsymbol{L}}_{\mathrm{e}}]^{\mathrm{sym}}, \quad \mathrm{D}_t\widehat{\boldsymbol{E}}_{\mathrm{k}} = -[\widehat{\boldsymbol{K}} \cdot \widehat{\boldsymbol{L}}_{\mathrm{k}}]^{\mathrm{sym}}, \quad \mathrm{D}_t\widehat{\boldsymbol{A}}^{-1} = 2\,[\widehat{\boldsymbol{L}}_{\mathrm{a}} \cdot \widehat{\boldsymbol{A}}^{-1}]^{\mathrm{sym}}, \tag{16}$$

whereby the notation $[\bullet]^{\mathrm{sym}}$ denotes the symmetric part of the second order field $\bullet$, e.g. $2[\widehat{\boldsymbol{C}}_{\mathrm{e}} \cdot \widehat{\boldsymbol{L}}_{\mathrm{e}}]^{\mathrm{sym}} = \widehat{\boldsymbol{C}}_{\mathrm{e}} \cdot \widehat{\boldsymbol{L}}_{\mathrm{e}} + \widehat{\boldsymbol{L}}^{\mathrm{d}}_{\mathrm{e}} \cdot \widehat{\boldsymbol{C}}_{\mathrm{e}}$. With these considerations at hand, the dissipation inequality (15) is rewritten as

$$\mathscr{D} = \widehat{\boldsymbol{M}}^{\mathrm{d}}_{\mathrm{e}} : \widehat{\boldsymbol{L}}_{\mathrm{p}} + \widehat{\boldsymbol{M}}^{\mathrm{d}}_{\mathrm{k}} : \widehat{\boldsymbol{L}}_{\mathrm{k}} - \widehat{\boldsymbol{M}}^{\mathrm{d}}_{\mathrm{a}} : \widehat{\boldsymbol{L}}_{\mathrm{a}} - Y\mathrm{D}_t\kappa \geqslant 0, \tag{17}$$

whereby the symmetry of the derivatives of the free Helmholtz energy density ψ with respect to $\widehat{\boldsymbol{E}}_{\mathrm{e}}$, $\widehat{\boldsymbol{E}}_{\mathrm{k}}$, $\widehat{\boldsymbol{A}}^{-1}$ has been applied and, following the standard argumentation of rational thermodynamics, the definition of the incorporated stress fields reads in detail

$$\widehat{\boldsymbol{M}}^{\mathrm{d}}_{\mathrm{e}} \doteq \widehat{\boldsymbol{C}}_{\mathrm{e}} \cdot \partial_{\widehat{\boldsymbol{E}}_{\mathrm{e}}}\psi_{\mathrm{e}}, \quad \widehat{\boldsymbol{M}}^{\mathrm{d}}_{\mathrm{k}} = \widehat{\boldsymbol{K}} \cdot \partial_{\widehat{\boldsymbol{E}}_{\mathrm{k}}}\psi_{\mathrm{k}}, \quad \widehat{\boldsymbol{M}}^{\mathrm{d}}_{\mathrm{a}} = 2\partial_{\widehat{\boldsymbol{A}}^{-1}}[\psi_{\mathrm{e}} + \psi_{\mathrm{k}}] \cdot \widehat{\boldsymbol{A}}^{-1}, \quad Y \doteq \partial_{\kappa}\psi_{\kappa}. \tag{18}$$

Remark 3.1. Even though the introduction of fictitious configurations whose underlying linear tangent maps define internal variables that account for degradation and kinematic hardening may seem somehow artificial, we observe that the model includes well-established formulations of finite inelasticity if specific kinematic assumptions are incorporated. Choosing, e.g., $\boldsymbol{F}_{\mathrm{a}}$ to be throughout represented by the identity, i.e. no degradation takes place and the model reflects the behavior of an elastically isotropic material, and replacing the introduced strain measure by the appropriate metric tensor results in the standard format $\psi_{\mathrm{e}} = \psi_{\mathrm{e}}(\widehat{\boldsymbol{C}}_{\mathrm{e}}, \widehat{\boldsymbol{G}}^{-1}; \boldsymbol{X}) = \psi_{\mathrm{e}}(\boldsymbol{C}, \boldsymbol{B}_{\mathrm{p}}; \boldsymbol{X}) = \psi_{\mathrm{e}}(\boldsymbol{g}, \boldsymbol{b}_{\mathrm{e}}; \boldsymbol{X})$ with $\boldsymbol{B}_{\mathrm{p}} = \boldsymbol{f}_{\mathrm{p}} \star \widehat{\boldsymbol{G}}^{-1}$ being obvious. Alternatively, the representation $\psi_{\mathrm{e}} = \psi_{\mathrm{e}}(\widehat{\boldsymbol{C}}_{\mathrm{e}} \cdot \widehat{\boldsymbol{G}}^{-1}; \boldsymbol{X}) = \psi_{\mathrm{e}}(\boldsymbol{C} \cdot \boldsymbol{B}_{\mathrm{p}}; \boldsymbol{X}) = \psi_{\mathrm{e}}(\boldsymbol{g} \cdot \boldsymbol{b}_{\mathrm{e}}; \boldsymbol{X})$ can be applied, compare e.g. Miehe (1995) ($\widehat{\psi}_{\mathrm{macro}}$), Svendsen (1998) ($\psi_{\mathrm{E}}$) or Govindjee and Reese (1997) (ψ^{k}). However, for the second contribution with tensorial arguments, ψ_{k}, we additionally assume $\boldsymbol{F}_{\mathrm{k}} \equiv \boldsymbol{F}_{\mathrm{p}}$ and introduce the metric $\widehat{\boldsymbol{b}}_{\mathrm{k}} \doteq \boldsymbol{F}_{\mathrm{k}} \star \widehat{\boldsymbol{G}}^{-1}$ which enables us to end up with $\psi_{\mathrm{k}} = \psi_{\mathrm{k}}(\widehat{\boldsymbol{G}}, \widehat{\boldsymbol{b}}_{\mathrm{k}}; \boldsymbol{X}) = \psi_{\mathrm{k}}(\boldsymbol{C}_{\mathrm{p}}, \boldsymbol{G}^{-1};$

$\boldsymbol{X}) = \psi_{\mathrm{k}}(\boldsymbol{c}_{\mathrm{e}}, \boldsymbol{b}; \boldsymbol{X})$ with $\boldsymbol{C}_{\mathrm{p}} = \boldsymbol{f}_{\mathrm{p}} \star \widehat{\boldsymbol{G}}$ being obvious. The alternative representation reads $\psi_{\mathrm{k}} = \psi_{\mathrm{k}}(\widehat{\boldsymbol{G}} \cdot \widehat{\boldsymbol{b}}_{\mathrm{k}}; \boldsymbol{X}) = \psi_{\mathrm{k}}(\boldsymbol{C}_{\mathrm{p}} \cdot \boldsymbol{G}^{-1}; \boldsymbol{X}) = \psi_{\mathrm{k}}(\boldsymbol{c}_{\mathrm{e}} \cdot \boldsymbol{b}; \boldsymbol{X})$, compare Svendsen (1998) (ψ_{P}).

3.1. Non-standard dissipative materials

Next, following the standard framework, we introduce an admissible elastic domain with respect to the intermediate configuration

$$\mathbb{A} = \left\{ \left(\widehat{\boldsymbol{M}}^{\mathrm{d}}_{\mathrm{r}}, Y \right) \middle| {}^{\mathrm{yie}}\phi\left(\widehat{\boldsymbol{M}}^{\mathrm{d}}_{\mathrm{r}}, Y; \boldsymbol{X} \right) \leqslant 0 \right\} \quad \text{with } \widehat{\boldsymbol{M}}^{\mathrm{d}}_{\mathrm{r}} \doteq \widehat{\boldsymbol{M}}^{\mathrm{d}}_{\mathrm{e}} - \widehat{\boldsymbol{M}}^{\mathrm{d}}_{\mathrm{k}} \tag{19}$$

which is determined by a convex yield function ${}^{\mathrm{yie}}\phi(\widehat{\boldsymbol{M}}^{\mathrm{d}}_{\mathrm{r}}, Y; \boldsymbol{X}) \doteq {}^{\mathrm{pla}}\phi(\widehat{\boldsymbol{M}}^{\mathrm{d}}_{\mathrm{r}}; \boldsymbol{X}) + {}^{\mathrm{har}}\phi(Y; \boldsymbol{X})$. Apparently, the relative stress $\widehat{\boldsymbol{M}}^{\mathrm{d}}_{\mathrm{r}}$ is introduced such that this Mandel-type tensor takes the commonly applied format for the formulation of kinematic hardening. Moreover, we assume the existence of a dissipation potential of Lemaitre-type, see e.g. Lemaitre and Chaboche (1998), namely

$${}^{\mathrm{pot}}\phi\left(\widehat{\boldsymbol{M}}^{\mathrm{d}}_{\mathrm{r}}, \widehat{\boldsymbol{M}}^{\mathrm{d}}_{\mathrm{a}}, Y; \boldsymbol{X} \right) \doteq {}^{\mathrm{yie}}\phi\left(\widehat{\boldsymbol{M}}^{\mathrm{d}}_{\mathrm{r}}, Y; \boldsymbol{X} \right) + {}^{\mathrm{dam}}\phi\left(\widehat{\boldsymbol{M}}^{\mathrm{d}}_{\mathrm{a}}; \boldsymbol{X} \right). \tag{20}$$

Based on these assumptions, appropriate evolution equations allow e.g. the following representation:

$$\begin{aligned}
&\widehat{\boldsymbol{L}}_{\mathrm{p}} \doteq \mathrm{D}_t\lambda\, \partial_{\widehat{\boldsymbol{M}}^{\mathrm{d}}_{\mathrm{e}}} {}^{\mathrm{pot}}\phi = \mathrm{D}_t\lambda\, \partial_{\widehat{\boldsymbol{M}}^{\mathrm{d}}_{\mathrm{e}}} {}^{\mathrm{pla}}\phi \doteq \mathrm{D}_t\lambda\, \widehat{\boldsymbol{v}}_{\mathrm{p}}, \\
&\widehat{\boldsymbol{L}}_{\mathrm{k}} \doteq \mathrm{D}_t\lambda\, \partial_{\widehat{\boldsymbol{M}}^{\mathrm{d}}_{\mathrm{k}}} {}^{\mathrm{pot}}\phi = \mathrm{D}_t\lambda\, \partial_{\widehat{\boldsymbol{M}}^{\mathrm{d}}_{\mathrm{k}}} {}^{\mathrm{pla}}\phi \doteq \mathrm{D}_t\lambda\, \widehat{\boldsymbol{v}}_{\mathrm{k}}, \\
&-\widehat{\boldsymbol{L}}_{\mathrm{a}} \doteq \mathrm{D}_t\lambda\, \partial_{\widehat{\boldsymbol{M}}^{\mathrm{d}}_{\mathrm{a}}} {}^{\mathrm{pot}}\phi = \mathrm{D}_t\lambda\, \partial_{\widehat{\boldsymbol{M}}^{\mathrm{d}}_{\mathrm{a}}} {}^{\mathrm{dam}}\phi \doteq \mathrm{D}_t\lambda\, \widehat{\boldsymbol{v}}_{\mathrm{a}}, \\
&-\mathrm{D}_t\kappa \doteq \mathrm{D}_t\lambda\, \partial_Y {}^{\mathrm{pot}}\phi = \mathrm{D}_t\lambda\, \partial_Y {}^{\mathrm{har}}\phi \doteq \mathrm{D}_t\lambda\, v_\kappa,
\end{aligned} \tag{21}$$

whereby the Lagrange multiplier $\mathrm{D}_t\lambda$ is either restricted by the conditions $\mathrm{D}_t\lambda > 0$, $\mathrm{D}_t\lambda\ {}^{\mathrm{yie}}\phi = 0$, $\mathrm{D}_t\lambda\ \mathrm{D}_t{}^{\mathrm{yie}}\phi = 0$ or, for a viscoplastic setting, determined via $t_{\mathrm{rel}}\ \mathrm{D}_t\lambda \doteq \eta({}^{\mathrm{yie}}\phi)$ with $t_{\mathrm{rel}} > 0$ and $\eta \in C^1 \,|\, \eta({}^{\mathrm{yie}}\phi \leqslant 0) = 0$ being a monotonically increasing functional. Obviously, we deal with associated evolution equations for the plasticity and hardening contributions but the damage part, nevertheless, remains non-associated.

Remark 3.2. Different types of kinematic hardening are commonly applied in elastoplasticity, e.g. Prager–, Ziegler– or Armstrong–Frederick equations which are, in contrast to the present formulation, frequently combined with the assumption of elastic isotropy. Even though the proposed finite strain framework monitors a similar setup than linear kinematic hardening within a small strain setting, its extension to e.g. nonlinear Armstrong–Frederick-type hardening is potentially included; compare e.g. Haupt (2000), Diegele et al. (2000) or Svendsen (1998) and Svendsen et al. (1998) for a detailed discussion. In this context, we obtain the classical non-associated format for the evolution of the Mandel-type back-stress tensor as $\mathrm{L}^{\mathrm{p}}_t \widehat{\boldsymbol{M}}^{\mathrm{d}}_{\mathrm{k}} \doteq c\, \widehat{\boldsymbol{L}}^{\mathrm{d}}_{\mathrm{p}} - b\, \mathrm{D}_t\lambda\, \widehat{\boldsymbol{M}}^{\mathrm{d}}_{\mathrm{k}}$ with $\mathrm{L}^{\mathrm{p}}_t[\bullet] = \boldsymbol{F}_{\mathrm{p}} \star \mathrm{D}_t(\boldsymbol{f}_{\mathrm{p}} \star [\bullet])$ denoting the Lie-derivative

with respect to the intermediate configuration. Moreover, non-associated saturation-type hardening is conveniently introduced via an extension of the corresponding evolution equation for $\boldsymbol{F}_{\mathrm{k}}$, namely $\widehat{\boldsymbol{L}}_{\mathrm{k}} \doteq \mathrm{D}_t\lambda[\widehat{\boldsymbol{v}}_{\mathrm{k}} + a\, K_{\infty}^{-1}\, \widehat{\boldsymbol{M}}_{\mathrm{k}}]$ with $K_{\infty} > 0$, see Ekh and Runesson (2001) for a comprehensive outline. Apparently, we apply this approach to the framework at hand and further details are given when needed, i.e. in Section 5.3.

Remark 3.3. In this work we place no emphasis on the introduction of any additional constitutive spin equation. Applications of plastic spin for a similar kinematic hardening formulation that is restricted to elastic isotropy without any degradation of the material is given by Wallin et al. (2003). For a general survey we refer the reader to Dafalias (1998) and the contributions by Cleja-Ţigoiu (2000), Tsakmakis (2004), Häusler et al. (2004), Haupt and Kersten (2003) and Paulun and Ręcherski (1992).

3.2. Constitutive integrator

Concerning the numerical integration technique for the obtained evolution equations, the time domain of interest is subdivided into several intervals; $\mathbb{T} = \bigcup_{n=0}^{N} [t^n, t^{n+1}]$ with $\Delta t \doteq t^{n+1} - t^n > 0$ being obvious. Now, from Eqs. (12) and (21) and following the approach as advocated by Weber and Anand (1990), we obtain the relation

$$\boldsymbol{F}_{\mathrm{p}}^{n+1} \doteq \exp(\Delta\lambda\, \widehat{\boldsymbol{v}}_{\mathrm{p}}^{n+1}) \cdot \boldsymbol{F}_{\mathrm{p}}^{n} \Rightarrow \boldsymbol{F}_{\mathrm{e}}^{n+1} = \boldsymbol{F}_{\mathrm{tri}} \cdot \exp(-\Delta\lambda\, \widehat{\boldsymbol{v}}_{\mathrm{p}}^{n+1}) \tag{22}$$

with $\boldsymbol{F}_{\mathrm{tri}} = \boldsymbol{F}^{n+1} \cdot \boldsymbol{f}_{\mathrm{p}}^{n}$. It turns out that $\widehat{\boldsymbol{v}}_{\mathrm{p}}$ is generally non-symmetric since we do not consider any specific restrictions to isotropy. In complete analogy, an exponential integration scheme can be applied to the kinematic hardening and the damage contribution

$$\boldsymbol{F}_{\mathrm{k}}^{n+1} \doteq \exp(\Delta\lambda\, \widehat{\boldsymbol{v}}_{\mathrm{k}}^{n+1}) \cdot \boldsymbol{F}_{\mathrm{k}}^{n}, \quad \boldsymbol{F}_{\mathrm{a}}^{n+1} \doteq \exp(-\Delta\lambda\, \widehat{\boldsymbol{v}}_{\mathrm{a}}^{n+1}) \cdot \boldsymbol{F}_{\mathrm{a}}^{n}, \tag{23}$$

recall Eq. (13), while an Euler backward approach may serve as integration rule for the hardening variable; i.e. $\kappa^{n+1} \doteq \kappa^n - \Delta\lambda\, v_{\kappa}^{n+1}$. Once more, it is the anisotropic material behavior that causes generally non-symmetric flow directions $\widehat{\boldsymbol{v}}_{\mathrm{k}}$ and $\widehat{\boldsymbol{v}}_{\mathrm{a}}$. These implicit integration rules result in a nonlinear system of equations which is represented by the following residua

$$\begin{aligned}
\boldsymbol{R}_{\mathrm{e}} &= \boldsymbol{F}_{\mathrm{e}}^{n+1} - \boldsymbol{F}_{\mathrm{e}}^{\mathrm{tri}} \cdot \exp(-\Delta\lambda\, \widehat{\boldsymbol{v}}_{\mathrm{p}}^{n+1}),\\
\boldsymbol{R}_{\mathrm{k}} &= \boldsymbol{F}_{\mathrm{k}}^{n+1} - \exp(\Delta\lambda\, \widehat{\boldsymbol{v}}_{\mathrm{k}}^{n+1}) \cdot \boldsymbol{F}_{\mathrm{k}}^{n},\\
\boldsymbol{R}_{\mathrm{a}} &= \boldsymbol{F}_{\mathrm{a}}^{n+1} - \exp(-\Delta\lambda\, \widehat{\boldsymbol{v}}_{\mathrm{d}}^{n+1}) \cdot \boldsymbol{F}_{\mathrm{a}}^{n},\\
R_{\kappa} &= \kappa^{n+1} - \kappa^{n} + \Delta\lambda\, v_{\kappa}^{n+1},
\end{aligned} \tag{24}$$

which determine the Jacobian of a typical Newton-type iteration scheme, namely

$$\begin{bmatrix} \partial_{\boldsymbol{F}_{\mathrm{e}}^{n+1}}\boldsymbol{R}_{\mathrm{e}} & \partial_{\boldsymbol{F}_{\mathrm{k}}^{n+1}}\boldsymbol{R}_{\mathrm{e}} & \partial_{\boldsymbol{F}_{\mathrm{a}}^{n+1}}\boldsymbol{R}_{\mathrm{e}} & \\ \partial_{\boldsymbol{F}_{\mathrm{e}}^{n+1}}\boldsymbol{R}_{\mathrm{k}} & \partial_{\boldsymbol{F}_{\mathrm{k}}^{n+1}}\boldsymbol{R}_{\mathrm{k}} & \partial_{\boldsymbol{F}_{\mathrm{a}}^{n+1}}\boldsymbol{R}_{\mathrm{k}} & \\ \partial_{\boldsymbol{F}_{\mathrm{e}}^{n+1}}\boldsymbol{R}_{\mathrm{a}} & \partial_{\boldsymbol{F}_{\mathrm{k}}^{n+1}}\boldsymbol{R}_{\mathrm{a}} & \partial_{\boldsymbol{F}_{\mathrm{a}}^{n+1}}\boldsymbol{R}_{\mathrm{a}} & \\ & & & \partial_{\kappa^{n+1}}R_{\kappa} \end{bmatrix} \circ \begin{bmatrix} \Delta\boldsymbol{F}_{\mathrm{e}} \\ \Delta\boldsymbol{F}_{\mathrm{k}} \\ \Delta\boldsymbol{F}_{\mathrm{a}} \\ \Delta\kappa \end{bmatrix} = \begin{bmatrix} -\boldsymbol{R}_{\mathrm{e}} \\ -\boldsymbol{R}_{\mathrm{k}} \\ -\boldsymbol{R}_{\mathrm{a}} \\ -R_{\kappa} \end{bmatrix}, \tag{25}$$

whereby the notation $\circ$ abbreviates the appropriate contraction operation. It turns out that these 'local' Jacobians, as well as the 'global' Jacobian or rather the algorithmic tangent operator within a finite element setting, can be conveniently approximated via a first order difference perturbation scheme. For a detailed outline of the underlying algorithm we refer the reader to the monograph by Dennis and Schnabel (1996) and Miehe (1996b) or Menzel and Steinmann (2003a), see also the contributions by Pérez-Foguet et al. (2000a,b) or Fellin and Ostermann (2002) which refer to a small strain setting. The computation of the Lagrange multiplier follows either from the solution of the nonlinear equation ${}^{\mathrm{yie}}\phi^{n+1}(\Delta\lambda,\ldots)\doteq 0$ or by seeking the solution of the nonlinear relation $t_{\mathrm{rel}}\,\Delta\lambda - \Delta t\,\eta^{n+1}(\Delta\lambda,\ldots)\doteq 0$, with $\Delta\lambda \equiv \Delta t\,\mathrm{D}_t\lambda$ being obvious (recall that $t_{\mathrm{rel}}\to 0$ leads to $\eta^{n+1}\to 0$ and ${}^{\mathrm{yie}}\phi^{n+1}\to 0$, i.e. recovers the rate-independent case). We choose in particular a staggered scheme where any convenient scalar-valued iteration can be applied to the calculation of the Lagrange multiplier. A brief summary is given in Algorithm 3.1.

Algorithm 3.1. Staggered solution technique: Newton-type algorithm to solve the set of nonlinear equations for $\boldsymbol{F}_{\mathrm{e}}^{n+1}$, $\boldsymbol{F}_{\mathrm{k}}^{n+1}$, $\boldsymbol{F}_{\mathrm{a}}^{n+1}$ and κ^{n+1} embedded into a scalar-valued iteration to compute the Lagrange multiplier $\Delta\lambda$.

Finite Element Method
for given $\boldsymbol{F}^{n+1}$, $\boldsymbol{F}_{\mathrm{p}}^{n}$, $\boldsymbol{F}_{\mathrm{k}}^{n}$, $\boldsymbol{F}_{\mathrm{a}}^{n}$, κ^{n} **do**
if ${}^{\mathrm{yie}}\phi^{n+1} > 0$ **then**
scalar-valued iteration
dowhile $|\,\Delta\Delta\lambda\,| >$ tol
$\ldots$
$\Delta\lambda + \Delta\Delta\lambda \mapsto \Delta\lambda$
Newton-type iteration
dowhile $\|\boldsymbol{R}_{\mathrm{e}}\| + \|\boldsymbol{R}_{\mathrm{k}}\| + \|\boldsymbol{R}_{\mathrm{a}}\| + |\,R_{\kappa}\,| >$ tol
$\ldots$
$\boldsymbol{F}_{\mathrm{e}}^{n+1} + \Delta\boldsymbol{F}_{\mathrm{e}} \mapsto \boldsymbol{F}_{\mathrm{e}}^{n+1}$
$\boldsymbol{F}_{\mathrm{k}}^{n+1} + \Delta\boldsymbol{F}_{\mathrm{k}} \mapsto \boldsymbol{F}_{\mathrm{k}}^{n+1}$
$\boldsymbol{F}_{\mathrm{a}}^{n+1} + \Delta\boldsymbol{F}_{\mathrm{a}} \mapsto \boldsymbol{F}_{\mathrm{a}}^{n+1}$
$\kappa^{n+1} + \Delta\kappa \mapsto \kappa^{n+1}$
enddo
enddo
endif

Remark 3.4. Please note that the exponential of a generally non-symmetric second order tensor is performed via a series expansion since no spectral decomposition is conveniently available. Higher order powers thereby allow representation via the Cayley–Hamilton theorem which improves the numerical efficiency of the computation, compare Miehe (1996a). The specific case with the flow direction being the

product of two symmetric second order tensors (at least one of them positive definite), which results in a generalized eigenvalue problem, is discussed below; see Section 5.2.

4. Fictitious configuration concept

In the sequel we give a detailed outline of how the introduced fictitious configurations or rather the corresponding linear tangent maps shape the proposed formulation. The damage mapping $\boldsymbol{F}_{\mathrm{a}}$ thereby defines an energy metric with respect to the stress-free intermediate configuration of multiplicative elastoplasticity, namely $\widehat{\boldsymbol{A}}^{-1} = \boldsymbol{F}_{\mathrm{a}} \bigstar \bar{\boldsymbol{G}}^{-1} : T^{*}\mathscr{B}_{\mathrm{p}} \to T\mathscr{B}_{\mathrm{p}}$. Conceptually speaking, we deal with an Euclidian geometry which is based on a non-constant and possibly non-spherical metric that accounts for both anisotropy and degradation, see also Menzel and Steinmann (2003a) or Menzel et al. (2003).

4.1. Free Helmholtz energy density

The introduction of the free Helmholtz energy density was essentially based on an additive decomposition, $\psi \doteq \psi_{\mathrm{e}} + \psi_{\mathrm{k}} + \psi_{\kappa}$, and application of the general covariance principle, or rather adopting the concept of strain energy equivalence, enables us to give the following representation:

$$\begin{aligned}\psi &= \psi_{\mathrm{e}}(\bar{\boldsymbol{E}}_{\mathrm{e}}, \bar{\boldsymbol{G}}^{-1}; \boldsymbol{X}) + \psi_{\mathrm{k}}(\bar{\boldsymbol{E}}_{\mathrm{k}}, \bar{\boldsymbol{G}}^{-1}; \boldsymbol{X}) + \psi_{\kappa}(\kappa; \boldsymbol{X}) \\ &= \psi_{\mathrm{e}}(\widehat{\boldsymbol{E}}_{\mathrm{e}}, \widehat{\boldsymbol{A}}^{-1}; \boldsymbol{X}) + \psi_{\mathrm{k}}(\widehat{\boldsymbol{E}}_{\mathrm{k}}, \widehat{\boldsymbol{A}}^{-1}; \boldsymbol{X}) + \psi_{\kappa}(\kappa; \boldsymbol{X}).\end{aligned} \tag{26}$$

We restrict ourselves to an outline with respect to the intermediate and the, say, effective configuration, since transformations to other configurations are straightforward. As the key idea of the proposed framework, the fictitious configuration is assumed to represent an initially isotropic setting such that we consequently obtain a set of only three invariants for each of the contributions ψ_{e} and ψ_{k}, i.e.

$$\begin{aligned}I_{\mathrm{e}\,i} &= \bar{\boldsymbol{I}} : [\bar{\boldsymbol{E}}_{\mathrm{e}} \cdot \bar{\boldsymbol{G}}^{-1}]^{i} = \widehat{\boldsymbol{I}} : [\widehat{\boldsymbol{E}}_{\mathrm{e}} \cdot \widehat{\boldsymbol{A}}^{-1}]^{i}, \\ I_{\mathrm{k}\,i} &= \bar{\boldsymbol{I}} : [\bar{\boldsymbol{E}}_{\mathrm{k}} \cdot \bar{\boldsymbol{G}}^{-1}]^{i} = \widehat{\boldsymbol{I}} : [\widehat{\boldsymbol{E}}_{\mathrm{k}} \cdot \widehat{\boldsymbol{A}}^{-1}]^{i}\end{aligned} \tag{27}$$

with $i = 1, 2, 3$. Based on this, we observe from Eq. (18) that the Mandel-type stress tensors possess the relations

$$\begin{aligned}\widehat{\boldsymbol{M}}^{\mathrm{d}}_{\mathrm{e}} &= \sum_{i=1}^{3} i\, \partial_{I_{\mathrm{e}\,i}} \psi_{\mathrm{e}}\, \widehat{\boldsymbol{C}}_{\mathrm{e}} \cdot \widehat{\boldsymbol{A}}^{-1} \cdot [\widehat{\boldsymbol{E}}_{\mathrm{e}} \cdot \widehat{\boldsymbol{A}}^{-1}]^{i-1}, \\ \widehat{\boldsymbol{M}}^{\mathrm{d}}_{\mathrm{k}} &= \sum_{i=1}^{3} i\, \partial_{I_{\mathrm{k}\,i}} \psi_{\mathrm{k}}\, \widehat{\boldsymbol{K}} \cdot \widehat{\boldsymbol{A}}^{-1} \cdot [\widehat{\boldsymbol{E}}_{\mathrm{k}} \cdot \widehat{\boldsymbol{A}}^{-1}]^{i-1}, \\ \widehat{\boldsymbol{M}}^{\mathrm{d}}_{\mathrm{a}} &= 2 \sum_{i=1}^{3} i \Big[\partial_{I_{\mathrm{e}\,i}} \psi_{\mathrm{e}}\, [\widehat{\boldsymbol{E}}_{\mathrm{e}} \cdot \widehat{\boldsymbol{A}}^{-1}]^{i} + \partial_{I_{\mathrm{k}\,i}} \psi_{\mathrm{k}}\, [\widehat{\boldsymbol{E}}_{\mathrm{k}} \cdot \widehat{\boldsymbol{A}}^{-1}]^{i} \Big] \\ &= 2 \widehat{\boldsymbol{E}}_{\mathrm{e}} \cdot \widehat{\boldsymbol{B}}_{\mathrm{e}} \cdot \widehat{\boldsymbol{M}}^{\mathrm{d}}_{\mathrm{e}} + 2\, \widehat{\boldsymbol{E}}_{\mathrm{k}} \cdot \widehat{\boldsymbol{K}}^{-1} \cdot \widehat{\boldsymbol{M}}^{\mathrm{d}}_{\mathrm{k}}\end{aligned} \tag{28}$$

and satisfy the following symmetry properties:

$$\widehat{\boldsymbol{M}}{}^{\mathrm{d}}_{\mathrm{e}} \cdot \widehat{\boldsymbol{C}}_{\mathrm{e}} = \widehat{\boldsymbol{C}}_{\mathrm{e}} \cdot \widehat{\boldsymbol{M}}_{\mathrm{e}}, \quad \widehat{\boldsymbol{M}}{}^{\mathrm{d}}_{\mathrm{k}} \cdot \widehat{\boldsymbol{K}} = \widehat{\boldsymbol{K}} \cdot \widehat{\boldsymbol{M}}_{\mathrm{k}}, \quad \widehat{\boldsymbol{A}}^{-1} \cdot \widehat{\boldsymbol{M}}{}^{\mathrm{d}}_{\mathrm{a}} = \widehat{\boldsymbol{M}}_{\mathrm{a}} \cdot \widehat{\boldsymbol{A}}^{-1}. \tag{29}$$

It turns out that the underlying kinematic assumptions, i.e. the affine pre-deformation characterized by $\boldsymbol{F}_{\mathrm{a}}$, result either in an isotropic setting or subclasses of transversal or orthotropic symmetry, see Menzel and Steinmann (2001a) for a detailed discussion. It is obvious, that the contribution $\psi_\kappa(\kappa;\boldsymbol{X})$ is not affected by the fictitious configuration concept, since only scalar-valued arguments are incorporated.

Remark 4.1. Even for isotropic or rather proportional hardening, which is represented in the proposed formulation by the scalar-valued internal variable κ, one could alternatively introduce a tensorial field of second order, see Menzel et al. (2002).

Remark 4.2. The elastic second Piola–Kirchhoff-type stress tensors are defined via $\widehat{\boldsymbol{S}}_{\mathrm{e}} \doteq \partial_{\widehat{\boldsymbol{E}}_{\mathrm{e}}} \psi_{\mathrm{e}} = \widehat{\boldsymbol{b}}_{\mathrm{e}} \cdot \widehat{\boldsymbol{M}}{}^{\mathrm{d}}_{\mathrm{e}}$ and $\bar{\boldsymbol{S}}_{\mathrm{e}} = \boldsymbol{f}_{\mathrm{a}} \bigstar \widehat{\boldsymbol{S}}_{\mathrm{e}} = \boldsymbol{f}_{\mathrm{a}} \cdot \widehat{\boldsymbol{S}}_{\mathrm{e}} \cdot \boldsymbol{f}{}^{\mathrm{d}}_{\mathrm{a}}$, respectively. Similarly, we introduce in view of the kinematic hardening contribution the stress field $\widehat{\boldsymbol{S}}_{\mathrm{k}} \doteq \partial_{\widehat{\boldsymbol{E}}_{\mathrm{k}}} \psi_{\mathrm{k}} = \widehat{\boldsymbol{K}}^{-1} \cdot \widehat{\boldsymbol{M}}{}^{\mathrm{d}}_{\mathrm{k}}$ and $\bar{\boldsymbol{S}}_{\mathrm{k}} = \boldsymbol{f}_{\mathrm{a}} \bigstar \widehat{\boldsymbol{S}}_{\mathrm{k}} = \boldsymbol{f}_{\mathrm{a}} \cdot \widehat{\boldsymbol{S}}_{\mathrm{k}} \cdot \boldsymbol{f}{}^{\mathrm{d}}_{\mathrm{a}}$. The Cauchy stress however, which e.g. enters the underlying balance of linear momentum, is obtained from Eq. (28) via pushforward operation, i.e. $\boldsymbol{\sigma}_{\mathrm{e}} = \det{}^{-1}(\boldsymbol{F})\, \boldsymbol{F}_{\mathrm{e}} \bigstar \widehat{\boldsymbol{S}}_{\mathrm{e}} = \det{}^{-1}(\boldsymbol{F}) \sum_{i=1}^{3} i\, \partial_{I_{\mathrm{e}i}} \psi_{\mathrm{e}} \boldsymbol{a}^{-1} \cdot [\boldsymbol{e}_{\mathrm{e}} \cdot \boldsymbol{a}^{-1}]^{i-1}$ introducing the spatial energy metric $\boldsymbol{a}^{-1} = \boldsymbol{F}_{\mathrm{e}} \bigstar \boldsymbol{A}^{-1} = \boldsymbol{F}_{\mathrm{e}} \cdot \boldsymbol{A}^{-1} \cdot \boldsymbol{F}{}^{\mathrm{d}}_{\mathrm{e}}$ and the Almansi-type elastic strain measure $\boldsymbol{e}_{\mathrm{e}} = \boldsymbol{F}_{\mathrm{e}} \bigstar \widehat{\boldsymbol{E}}_{\mathrm{e}} = \frac{1}{2}[\boldsymbol{g} - \boldsymbol{c}_{\mathrm{e}}]$. The corresponding definition of the deviatoric Cauchy stress reads $\boldsymbol{\sigma}{}^{\mathrm{dev}}_{\mathrm{e}} \doteq \boldsymbol{\sigma}_{\mathrm{e}} - \frac{1}{3}[\boldsymbol{g} : \boldsymbol{\sigma}_{\mathrm{e}}]\boldsymbol{g}^{-1}$ (note that the spatial format of the incorporated invariants reads $I_{\mathrm{e}i} = \boldsymbol{i} : [\boldsymbol{e}_{\mathrm{e}} \cdot \boldsymbol{a}^{-1}]^i$, $i = 1, 2, 3$).

4.2. Damage potential

The same concept is now adopted for the damage potential, i.e. we assume ${}^{\mathrm{dam}}\phi(\bar{\boldsymbol{M}}{}^{\mathrm{d}}_{\mathrm{a}};\boldsymbol{X}) \doteq {}^{\mathrm{dam}}\phi(\widehat{\boldsymbol{M}}{}^{\mathrm{d}}_{\mathrm{a}};\boldsymbol{X})$ with

$$\begin{aligned} \bar{\boldsymbol{M}}{}^{\mathrm{d}}_{\mathrm{a}} &= \boldsymbol{f}_{\mathrm{a}} \bigstar \widehat{\boldsymbol{M}}{}^{\mathrm{d}}_{\mathrm{a}} = \boldsymbol{F}{}^{\mathrm{d}}_{\mathrm{a}} \cdot \widehat{\boldsymbol{M}}{}^{\mathrm{d}}_{\mathrm{a}} \cdot \boldsymbol{f}{}^{\mathrm{d}}_{\mathrm{a}} = 2\partial_{\bar{\boldsymbol{G}}^{-1}}[\psi_{\mathrm{e}} + \psi_{\mathrm{k}}] \cdot \bar{\boldsymbol{G}}^{-1} \\ &= 2\sum_{i=1}^{3} i\Big[\partial_{I_{\mathrm{e}i}} \psi_{\mathrm{e}} [\bar{\boldsymbol{E}}_{\mathrm{e}} \cdot \bar{\boldsymbol{G}}^{-1}]^i + \partial_{I_{\mathrm{k}i}} \psi_{\mathrm{k}} [\bar{\boldsymbol{E}}_{\mathrm{k}} \cdot \bar{\boldsymbol{G}}^{-1}]^i\Big], \end{aligned} \tag{30}$$

compare Eq. (18). In analogy to the fictitious configuration representing an initially isotropic setting, let the damage potential be determined via the following three invariants

$$I_{\mathrm{a}i} = \bar{\boldsymbol{I}} : [2\partial_{\bar{\boldsymbol{G}}^{-1}} \psi \cdot \bar{\boldsymbol{G}}^{-1}]^i = \bar{\boldsymbol{I}} : [\bar{\boldsymbol{M}}{}^{\mathrm{d}}_{\mathrm{a}}]^i = \widehat{\boldsymbol{I}} : [\widehat{\boldsymbol{M}}{}^{\mathrm{d}}_{\mathrm{a}}]^i = \widehat{\boldsymbol{I}} : [2\partial_{\widehat{\boldsymbol{A}}^{-1}} \psi \cdot \widehat{\boldsymbol{A}}^{-1}]^i \tag{31}$$

with $i = 1, 2, 3$. Conceptually speaking, the definition of these invariants is based on a symmetric stress field ($2\partial_{\bar{\boldsymbol{G}}^{-1}}[\psi_{\mathrm{e}} + \psi_{\mathrm{k}}]$ and $2\partial_{\widehat{\boldsymbol{A}}^{-1}}[\psi_{\mathrm{e}} + \psi_{\mathrm{k}}]$) with respect to the

appropriate metric ($\bar{\boldsymbol{G}}^{-1}$ and $\widehat{\boldsymbol{A}}^{-1}$). We consequently obtain for the related flow direction

$$\widehat{\boldsymbol{v}}_{\mathrm{a}} = \sum_{i=1}^{3} i\,\partial_{I_{\mathrm{a}\,i}}{}^{\mathrm{dam}}\phi[\widehat{\boldsymbol{M}}_{\mathrm{a}}]^{i-1} = \sum_{i=1}^{3} i\,\partial_{I_{\mathrm{a}\,i}}{}^{\mathrm{dam}}\phi\left[2\widehat{\boldsymbol{A}}^{-1}\cdot\partial_{\widehat{\boldsymbol{A}}^{-1}}[\psi_{\mathrm{e}}+\psi_{\mathrm{k}}]\right]^{i-1} \tag{32}$$

which results in connection with Eqs. (16) and (21) in the following remarkable result:

$$\begin{aligned}\mathrm{D}_t\widehat{\boldsymbol{A}}^{-1} &= 2[\widehat{\boldsymbol{L}}_{\mathrm{a}}\cdot\widehat{\boldsymbol{A}}^{-1}]^{\mathrm{sym}} = 2\widehat{\boldsymbol{L}}_{\mathrm{a}}\cdot\widehat{\boldsymbol{A}}^{-1} = -2\mathrm{D}_t\lambda\widehat{\boldsymbol{v}}_{\mathrm{a}}\cdot\widehat{\boldsymbol{A}}^{-1}\\ &= -2\mathrm{D}_t\lambda\sum_{i=1}^{3} i\,\partial_{I_{\mathrm{a}\,i}}{}^{\mathrm{dam}}\phi\,\widehat{\boldsymbol{A}}^{-1}\cdot[\widehat{\boldsymbol{M}}_{\mathrm{a}}^{\mathrm{d}}]^{i-1}.\end{aligned} \tag{33}$$

Practically speaking, the covariance principle in the present context yields $\widehat{\boldsymbol{L}}_{\mathrm{a}}$ to be generally symmetric with respect to $\widehat{\boldsymbol{A}}^{-1}$. Next, applying pullback operations to the damage contributions in the dissipation inequality (15) and (17) with respect to the fictitious configuration result in

$$\begin{aligned}&\partial_{\widehat{\boldsymbol{A}}^{-1}}\psi : \mathrm{D}_t\widehat{\boldsymbol{A}}^{-1} = \partial_{\bar{\boldsymbol{G}}^{-1}}\psi : \mathrm{l}_t^{\mathrm{a}}\bar{\boldsymbol{G}}^{-1} = \bar{\boldsymbol{M}}_{\mathrm{a}}^{\mathrm{d}} : \bar{\boldsymbol{L}}_{\mathrm{a}} = \widehat{\boldsymbol{M}}_{\mathrm{a}}^{\mathrm{d}} : \widehat{\boldsymbol{L}}_{\mathrm{a}} \quad \text{with}\\ &\mathrm{l}_t^{\mathrm{a}}\bar{\boldsymbol{G}}^{-1} = \boldsymbol{f}_{\mathrm{a}}\bigstar\mathrm{D}_t\widehat{\boldsymbol{A}}^{-1} = 2[\bar{\boldsymbol{L}}_{\mathrm{a}}\cdot\bar{\boldsymbol{G}}^{-1}]^{\mathrm{sym}}, \quad \bar{\boldsymbol{G}}^{-1} = \boldsymbol{f}_{\mathrm{a}}\bigstar\widehat{\boldsymbol{A}}^{-1},\end{aligned} \tag{34}$$

whereby the notation $\mathrm{l}_t^{\mathrm{a}}$ takes the interpretation as a Lie-derivative with respect to $\boldsymbol{f}_{\mathrm{a}}$, i.e. $\mathrm{l}_t^{\mathrm{a}}[\bullet] = \boldsymbol{f}_{\mathrm{a}}\bigstar\mathrm{D}_t(\boldsymbol{F}_{\mathrm{a}}\bigstar[\bullet])$. Furthermore, a pullback of the velocity gradient $\bar{\boldsymbol{L}}_{\mathrm{a}}$ yields

$$\bar{\boldsymbol{L}}_{\mathrm{a}} = \boldsymbol{f}_{\mathrm{a}}\bigstar\widehat{\boldsymbol{L}}_{\mathrm{a}} = \boldsymbol{f}_{\mathrm{a}}\cdot\mathrm{D}_t\boldsymbol{F}_{\mathrm{a}} = -\mathrm{D}_t\boldsymbol{f}_{\mathrm{a}}\cdot\boldsymbol{F}_{\mathrm{a}}, \tag{35}$$

compare Eq. (13). In analogy to Eqs. (23) and (33), an exponential integration scheme with respect to $\bar{\boldsymbol{L}}_{\mathrm{a}}$ ends up in the equivalent expression

$$\begin{aligned}\boldsymbol{F}_{\mathrm{a}}^{n+1} \doteq \boldsymbol{F}_{\mathrm{a}}^{n}\cdot\exp(-\Delta\lambda\bar{\boldsymbol{v}}_{\mathrm{a}}^{n+1}) \quad &\text{with } \bar{\boldsymbol{v}}_{\mathrm{a}} = \boldsymbol{f}_{\mathrm{a}}\bigstar\widehat{\boldsymbol{v}}_{\mathrm{a}} = \mathrm{D}_t\lambda\partial_{\bar{\boldsymbol{M}}_{\mathrm{a}}^{\mathrm{d}}}{}^{\mathrm{dam}}\phi\\ &= \mathrm{D}_t\lambda\sum_{i=1}^{3} i\,\partial_{I_{\mathrm{a}\,i}}{}^{\mathrm{dam}}\phi[\bar{\boldsymbol{M}}_{\mathrm{a}}]^{i-1}.\end{aligned} \tag{36}$$

Moreover, we can apply the spectral decomposition theorem to the Mandel-type stress tensors since these mixed-variant fields are composed by the product of two symmetric fields with one of these second order tensors always remaining positive definite, see e.g. Ericksen (1960), Eringen (1971) or Lodge (1974) for a discussion.

Remark 4.3. The damage stress tensor (as represented in Eq. (30) with respect to the fictitious configuration) turns out to be symmetric, i.e. $\bar{\boldsymbol{M}}_{\mathrm{a}}^{\mathrm{t}} = \bar{\boldsymbol{G}}^{-1}\cdot\bar{\boldsymbol{M}}_{\mathrm{a}}^{\mathrm{d}}\cdot\bar{\boldsymbol{G}} = \bar{\boldsymbol{M}}_{\mathrm{a}}$ whereby the notation t characterizes transposition.

4.3. Yield function

While the approaches for the free Helmholtz energy density and the damage potential are conceptually established as the postulate of strain energy equivalence,

as e.g. discussed by Sidoroff (1981), attention is now paid to the postulate of strain equivalence as commonly applied to the coupling of plasticity and continuum damage, see e.g. Steinmann et al. (1994) or Lämmer and Tsakmakis (2000) where several coupling-types of isotropic continuum damage and plasticity are highlighted. In this direction, we introduce with a small abuse of notation an effective elastic Mandel stress tensor

$$^{\text{eff}}\widehat{\boldsymbol{M}}^{\text{d}}_{\text{e}} \equiv [\boldsymbol{f}^{\text{d}}_{\text{a}} \cdot \widehat{\boldsymbol{C}}_{\text{e}} \cdot \boldsymbol{f}_{\text{a}}] \cdot \partial_{\widehat{\boldsymbol{E}}_{\text{e}}} \psi_{\text{e}}, \quad ^{\text{eff}}\widehat{\boldsymbol{M}}^{\text{d}}_{\text{e}} \cdot \widehat{\boldsymbol{C}}_{\text{e}} \neq \widehat{\boldsymbol{C}}_{\text{e}} \cdot ^{\text{eff}}\widehat{\boldsymbol{M}}_{\text{e}}. \tag{37}$$

The underlying kinematics are essentially based on the assumption $^{\text{eff}}\bar{\boldsymbol{M}}^{\text{d}}_{\text{e}} = \boldsymbol{f}_{\text{a}} \bigstar ^{\text{eff}}\widehat{\boldsymbol{M}}^{\text{d}}_{\text{e}} \equiv \widehat{\boldsymbol{C}}_{\text{e}} \cdot \bar{\boldsymbol{S}}_{\text{e}}$, i.e. the effective elastic Mandel tensor is defined by the composition of an appropriate stress field and a modified metric tensor that accounts for the anisotropic degradation of the material, compare Remark 4.2. A detailed discussion on the application of the equivalent strain concept within the present context is given in Menzel and Steinmann (2003a). With this effective quantity at hand, the yield function is assumed to be determined via an effective relative Mandel stress tensor

$$^{\text{yie}}\phi \doteq ^{\text{yie}}\phi(^{\text{eff}}\widehat{\boldsymbol{M}}^{\text{d}}_{\text{r}}, Y; \boldsymbol{X}) \quad \text{with } ^{\text{eff}}\widehat{\boldsymbol{M}}^{\text{d}}_{\text{r}} = ^{\text{eff}}\widehat{\boldsymbol{M}}^{\text{d}}_{\text{e}} - \widehat{\boldsymbol{M}}^{\text{d}}_{\text{k}}. \tag{38}$$

Apparently, we do not elaborate the influence of different effective stress measures, as e.g. the incorporation of an effective back-stress tensor, since this is not within the present scope of the present contribution; in this regard we refer the reader to the work by Lämmer and Tsakmakis (2000). However, straightforward application of the evolution equations as highlighted in Eq. (21) results in the following relations for the corresponding flow directions:

$$\begin{aligned}
\widehat{\boldsymbol{v}}_{\text{p}} &= \frac{\partial^{\text{pla}}\phi}{\partial^{\text{eff}}\widehat{\boldsymbol{M}}^{\text{d}}_{\text{r}}} : \frac{\partial^{\text{eff}}\widehat{\boldsymbol{M}}^{\text{d}}_{\text{r}}}{\partial\widehat{\boldsymbol{M}}^{\text{d}}_{\text{e}}} \equiv \frac{\partial^{\text{pla}}\phi}{\partial^{\text{eff}}\widehat{\boldsymbol{M}}^{\text{d}}_{\text{r}}} : \left[[\boldsymbol{f}^{\text{d}}_{\text{a}} \cdot \widehat{\boldsymbol{C}}_{\text{e}} \cdot \boldsymbol{f}_{\text{a}} \cdot \widehat{\boldsymbol{B}}_{\text{e}}] \overline{\otimes} \widehat{\boldsymbol{I}}\right], \\
\widehat{\boldsymbol{v}}_{\text{k}} &= \frac{\partial^{\text{pla}}\phi}{\partial^{\text{eff}}\widehat{\boldsymbol{M}}^{\text{d}}_{\text{r}}} : \frac{\partial^{\text{eff}}\widehat{\boldsymbol{M}}^{\text{d}}_{\text{r}}}{\partial\widehat{\boldsymbol{M}}^{\text{d}}_{\text{k}}} \equiv -\frac{\partial^{\text{pla}}\phi}{\partial^{\text{eff}}\widehat{\boldsymbol{M}}^{\text{d}}_{\text{r}}} : [\widehat{\boldsymbol{I}}^{\text{d}} \overline{\otimes} \widehat{\boldsymbol{I}}],
\end{aligned} \tag{39}$$

whereby the non-standard dyadic product is defined via $\boldsymbol{U} : [\boldsymbol{V} \overline{\otimes} \boldsymbol{W}] \doteq \boldsymbol{V}^{\text{d}} \cdot \boldsymbol{U} \cdot \boldsymbol{W}$ with $\boldsymbol{U}, \boldsymbol{W} : T\mathscr{B} \to T\mathscr{B}$, $\boldsymbol{V} : T^*\mathscr{B} \to T^*\mathscr{B}$ for some configuration $\mathscr{B}$. For conceptual clarity, the hardening contribution $^{\text{har}}\phi(Y; \boldsymbol{X})$ remains unchanged in this work, i.e. no further modifications with respect to the damage mapping are applied.

The following prototype model is introduced such that well-established constitutive equations are adopted as far as possible, e.g. a St.–Venant Kirchhoff ansatz or v. Mises-type yield functions. Both, the incorporation and examination of different prototype models as e.g. Neo–Hooke- or Hill-type models constitute future research. In that case, the identification of material parameters is of cardinal importance and a non-trivial task while the parameters for the prototype model chosen in this work are

rather settled. Based on this, we are able to run several numerical academic examples that monitor the general material behavior of the developed framework in a clear and reasonable fashion.

5.1. Free Helmholtz energy density

Based on the previously highlighted additive split of the free Helmholtz energy density we adopt a simple ansatz of St. Venant Kirchhoff type for the elastic and kinematic hardening contribution, i.e.

$$\psi_{\mathrm{e}} \doteq \frac{1}{2} L I_{\mathrm{e}1}^2 + G\, I_{\mathrm{e}2}, \quad \psi_{\mathrm{k}} \doteq H_3\, [I_{\mathrm{k}2} - \frac{1}{3} I_{\mathrm{k}1}^2] \tag{40}$$

with $G > 0$, $L > -\frac{2}{3} G$ and $H_3 > 0$. The chosen hardening contribution takes a standard format such that linear and saturation-type effects are modeled

$$\psi_{\kappa} \doteq [Y_\infty - Y_0][\kappa + H_1^{-1} \exp(-H_1 \kappa) - H_1^{-1}] + \frac{1}{2} H_2 \kappa^2 \tag{41}$$

and $H_{1,2} \geqslant 0$, $Y_\infty \geqslant Y_0 \geqslant 0$.

5.2. Damage potential

Since the fictitious configuration is assumed to represent an isotropic configuration, the damage potential ${}^{\mathrm{dam}}\phi$ can either by defined in terms of the highlighted basic invariants $I_{\mathrm{a}\,1,2,3}$, the corresponding principal invariants or the correlated eigenvalues of $\widehat{\boldsymbol{M}}_{\mathrm{a}}^{\mathrm{d}}$ or $\bar{\boldsymbol{M}}_{\mathrm{a}}^{\mathrm{d}}$, respectively – all of them being real (in the sequel we restrict ourselves to these two configurations even though an outline with respect to, e.g., $\mathscr{B}_0$ or $\mathscr{B}_t$ follows straightforward). Keeping a generalized eigenvalue problem in mind, the Mandel-type damage stress tensor can be decomposed as (recall Section 4.2)

$$\begin{aligned} \widehat{\boldsymbol{M}}_{\mathrm{a}}^{\mathrm{d}} &= \sum_{i=1}^{3} \lambda_{\mathrm{a}\,i} \widehat{\boldsymbol{n}}^i \otimes \widehat{\boldsymbol{n}}_i \quad \text{with } \|\widehat{\boldsymbol{n}}_i\|_{\widehat{\boldsymbol{A}}} = 1,\ \widehat{\boldsymbol{A}} = \sum_{i=1}^{3} \widehat{\boldsymbol{n}}^i \otimes \widehat{\boldsymbol{n}}^i, \\ \bar{\boldsymbol{M}}_{\mathrm{a}}^{\mathrm{d}} &= \sum_{i=1}^{3} \lambda_{\mathrm{a}\,i} \bar{\boldsymbol{n}}^i \otimes \bar{\boldsymbol{n}}_i \quad \text{with } \|\bar{\boldsymbol{n}}_i\|_{\bar{\boldsymbol{G}}} = 1,\ \bar{\boldsymbol{G}} = \sum_{i=1}^{3} \bar{\boldsymbol{n}}^i \otimes \bar{\boldsymbol{n}}^i \end{aligned} \tag{42}$$

with $\widehat{\boldsymbol{A}} = \boldsymbol{F}_{\mathrm{a}} \bigstar \bar{\boldsymbol{G}} = \boldsymbol{f}_{\mathrm{a}}^{\mathrm{d}} \cdot \bar{\boldsymbol{G}} \cdot \boldsymbol{f}_{\mathrm{a}}$ and $\widehat{\boldsymbol{n}}^i = \widehat{\boldsymbol{A}} \cdot \widehat{\boldsymbol{n}}_i$, $\bar{\boldsymbol{n}}^i = \bar{\boldsymbol{G}} \cdot \bar{\boldsymbol{n}}_i$ as well as $\widehat{\boldsymbol{n}}^i = \boldsymbol{f}_{\mathrm{a}}^{\mathrm{d}} \cdot \bar{\boldsymbol{n}}^i$, $\widehat{\boldsymbol{n}}_i = \boldsymbol{F}_{\mathrm{a}} \cdot \bar{\boldsymbol{n}}_i$ (and usually $\lambda_{\mathrm{a}\,1} \leqslant \lambda_{\mathrm{a}\,2} \leqslant \lambda_{\mathrm{a}\,3}$).

Based on this, the setup of a Rankine-type model is straightforward: Here we follow the outline given by Carol et al. (2001), further developed in Menzel et al. (2003), and introduce the damage potential

$${}^{\mathrm{dam}}\phi(\widehat{\boldsymbol{M}}_{\mathrm{a}}^{\mathrm{d}}; \boldsymbol{X}) = {}^{\mathrm{dam}}\phi(\bar{\boldsymbol{M}}_{\mathrm{a}}^{\mathrm{d}}; \boldsymbol{X}) \doteq \left[\sum_{i=1}^{3} \langle \lambda_{\mathrm{a}\,i} \rangle^{D+1} \right]^{\frac{1}{D+1}} \geqslant 0, \quad D \geqslant 0, \tag{43}$$

whereby the definition of the McCauley bracket reads $\langle \bullet \rangle = \frac{1}{2}[\bullet + | \bullet |]$, $\bullet \in \mathbb{R}$. For $D \to 0$ the presented model boils down to (quasi) isotropic damage while $D > 0$

yields an anisotropic damage formulation. However, independent of the specific choice of D different material behavior in, say, 'tension and compression' is modeled throughout (with respect to the space of the driving damage force). This concept is commonly applied in strain space, see e.g. Ekh et al. (2003b) for an outline in the present context. With this damage potential at hand, the computation of the corresponding flow-direction results in

$$\begin{aligned}\widehat{\boldsymbol{v}}_{\mathrm{a}} &= \sum_{i=1}^{3} {}^{\mathrm{dam}}\phi^{-D}\langle\lambda_{\mathrm{a}\,i}\rangle^{D}\,\mathscr{H}(\lambda_{\mathrm{a}\,i})\,\widehat{\boldsymbol{n}}_i\otimes\widehat{\boldsymbol{n}}^i,\\ \bar{\boldsymbol{v}}_{\mathrm{a}} &= \sum_{i=1}^{3} {}^{\mathrm{dam}}\phi^{-D}\langle\lambda_{\mathrm{a}\,i}\rangle^{D}\,\mathscr{H}(\lambda_{\mathrm{a}\,i})\,\bar{\boldsymbol{n}}_i\otimes\bar{\boldsymbol{n}}^i,\end{aligned} \tag{44}$$

see Eqs. (21), (32) and (36). Please recall the fundamental relation $I_{\mathrm{e}\,1}=\lambda_{\mathrm{a}\,1}+\lambda_{\mathrm{a}\,2}+\lambda_{\mathrm{a}\,3}$ and that $\partial_{\bullet}\langle\bullet\rangle$ equals the Heaviside function ($\mathscr{H}(\bullet)=1$ if $\bullet\geqslant 0$, $\mathscr{H}(\bullet)=0$ if $\bullet<0$ with $\bullet\in\mathbb{R}$) as well as the property $0\leqslant {}^{\mathrm{dam}}\phi^{-D}\ \langle\lambda_{\mathrm{a}\,i}\rangle^{D}\ \mathscr{H}(\lambda_{\mathrm{a}\,i})\leqslant 1$. Moreover, we immediately observe that the chosen damage model is thermodynamically consistent since the obtained contribution to the dissipation inequality always remains non-negative

$$\begin{aligned}-\widehat{\boldsymbol{M}}^{\mathrm{d}}_{\mathrm{a}}:\widehat{\boldsymbol{L}}_{\mathrm{a}} &= \sum_{i=1}^{3}\mathrm{D}_t\lambda_{\mathrm{a}\,i}\,{}^{\mathrm{dam}}\phi^{-D}\ \langle\lambda_{\mathrm{a}\,i}\rangle^{D}\,\mathscr{H}(\lambda_{\mathrm{a}\,i})[\widehat{\boldsymbol{n}}^i\otimes\widehat{\boldsymbol{n}}_i]:[\widehat{\boldsymbol{n}}_i\otimes\widehat{\boldsymbol{n}}^i]\geqslant 0,\\ -\bar{\boldsymbol{M}}^{\mathrm{d}}_{\mathrm{a}}:\bar{\boldsymbol{L}}_{\mathrm{a}} &= \sum_{i=1}^{3}\mathrm{D}_t\lambda_{\mathrm{a}\,i}\,{}^{\mathrm{dam}}\phi^{-D}\langle\lambda_{\mathrm{a}\,i}\rangle^{D}\,\mathscr{H}(\lambda_{\mathrm{a}\,i})[\bar{\boldsymbol{n}}^i\otimes\bar{\boldsymbol{n}}_i]:[\bar{\boldsymbol{n}}_i\otimes\bar{\boldsymbol{n}}^i]\geqslant 0,\end{aligned} \tag{45}$$

compare Eqs. (17), (21), (34).

Remark 5.1. Please note that the 'pseudo-logarithmic' damage rate as advocated in the work by Carol et al. (2001), where the adopted Rankine-type model is outlined for the coupling of linear elasticity and continuum damage mechanics, corresponds to the Lie-derivative $\mathrm{l}^{\mathrm{a}}_{t}$ introduced in Eq. (34). Moreover, neglecting the kinematic hardening contribution ψ_{k} the damage stress tensor allows representation as $\widehat{\boldsymbol{M}}^{\mathrm{d}}_{\mathrm{a}}=2\,\partial_{\widehat{\boldsymbol{A}}^{-1}}\psi_{\mathrm{e}}\cdot\widehat{\boldsymbol{A}}^{-1}=2\,\widehat{\boldsymbol{E}}_{\mathrm{e}}\cdot\partial_{\widehat{\boldsymbol{E}}_{\mathrm{e}}}\psi_{\mathrm{e}}=2\,\widehat{\boldsymbol{E}}_{\mathrm{e}}\cdot\widehat{\boldsymbol{S}}_{\mathrm{e}}$ or $\bar{\boldsymbol{M}}^{\mathrm{d}}_{\mathrm{a}}=2\,\bar{\boldsymbol{E}}_{\mathrm{e}}\cdot\bar{\boldsymbol{S}}_{\mathrm{e}}$, respectively. By comparing this result with Eq. (71) in Carol et al. (2001, Part I) we observe the relation $\widehat{\boldsymbol{M}}_{\mathrm{a}}\equiv-4\,\mathbf{Y}$.

5.3. Yield function

For the contribution ${}^{\mathrm{pla}}\phi$ of the yield function ${}^{\mathrm{yie}}\phi$, a well-established v. Mises-type model in connection with the concept of effective stress is adopted; we choose in particular

$$\begin{aligned}{}^{\mathrm{pla}}\phi &\doteq \sqrt{\frac{3}{2}}\left[\widehat{\boldsymbol{I}}:\left[\left[{}^{\mathrm{eff}}\widehat{\boldsymbol{M}}^{\mathrm{d}}_{\mathrm{r}}\right]^{\mathrm{dev}}\right]^{2}\right]^{\frac{1}{2}}\doteq\sqrt{\frac{3}{2}}\left[{}^{\mathrm{eff}}I^{\mathrm{dev}}_{\mathrm{p}\,2}\right]^{\frac{1}{2}}\quad\text{with }\left[{}^{\mathrm{eff}}\widehat{\boldsymbol{M}}^{\mathrm{d}}_{\mathrm{r}}\right]^{\mathrm{dev}}\\ &= {}^{\mathrm{eff}}\widehat{\boldsymbol{M}}^{\mathrm{d}}_{\mathrm{r}}-\frac{1}{3}\left[\widehat{\boldsymbol{I}}:{}^{\mathrm{eff}}\widehat{\boldsymbol{M}}^{\mathrm{d}}_{\mathrm{r}}\right]\widehat{\boldsymbol{I}}^{\mathrm{d}},\end{aligned} \tag{46}$$

which results in the following flow directions:

$$\widehat{\boldsymbol{v}}_{\mathrm{p}} = \frac{\partial^{\mathrm{pla}}\phi}{\partial \widehat{\boldsymbol{M}}^{\mathrm{d}}_{\mathrm{e}}} \equiv \sqrt{\frac{3}{2}}\big[{}^{\mathrm{eff}}\boldsymbol{I}^{\mathrm{dev}}_{\mathrm{p}\,2}\big]^{-\frac{1}{2}}\,\widehat{\boldsymbol{B}}_{\mathrm{e}}\cdot\boldsymbol{f}^{\mathrm{d}}_{\mathrm{a}}\cdot\widehat{\boldsymbol{C}}_{\mathrm{e}}\cdot\boldsymbol{f}_{\mathrm{a}}\cdot\big[{}^{\mathrm{eff}}\widehat{\boldsymbol{M}}_{\mathrm{r}}\big]^{\mathrm{dev}},$$
$$\widehat{\boldsymbol{v}}_{\mathrm{k}} = \frac{\partial^{\mathrm{pla}}\phi}{\partial \widehat{\boldsymbol{M}}^{\mathrm{d}}_{\mathrm{k}}} \equiv -\sqrt{\frac{3}{2}}\big[{}^{\mathrm{eff}}\boldsymbol{I}^{\mathrm{dev}}_{\mathrm{p}\,2}\big]^{-\frac{1}{2}}\big[{}^{\mathrm{eff}}\widehat{\boldsymbol{M}}_{\mathrm{r}}\big]^{\mathrm{dev}}, \tag{47}$$

recall Eq. (39). The adopted (linear) format of the hardening potential is the simplest possible, namely

$${}^{\mathrm{har}}\phi \doteq -\,[Y_0 + Y] \quad \text{such that } v_\kappa = -1. \tag{48}$$

The proof that the chosen v. Mises-type model is thermodynamically consistent is straightforward and therefore omitted. For a viscoplastic setting, the commonly applied Norton-type format or rather power law

$$\eta({}^{\mathrm{yie}}\phi) \doteq \left[\frac{\langle {}^{\mathrm{yie}}\phi\rangle}{Y_0}\right]^N \quad \text{with } N \geqslant 1 \tag{49}$$

is adopted. However, in order to account for nonlinear kinematic hardening we expand Eq. $(47)_2$ and assume

$$\widehat{\boldsymbol{v}}^{\mathrm{nonlin}}_{\mathrm{k}} = \widehat{\boldsymbol{v}}_{\mathrm{k}} + aK^{-1}_{\infty}\widehat{\boldsymbol{M}}_{\mathrm{k}} \quad \text{with } a \doteq \frac{3}{2}, \tag{50}$$

whereby K_∞ acts as a saturation value, recall Remark 3.2 and see Ekh and Runesson (2001) for a comprehensive outline.

5.4. Weighting of the evolution equations

In order to switch between different models, e.g. viscoplasticity coupled to anisotropic continuum damage without hardening effects or viscoplasticity with mixed hardening but without taking degradation into account, we introduce three weighting factors that scale the underlying evolution equations, namely

$$[1 - r_{\mathrm{k}}]\boldsymbol{v}_{\mathrm{k}} \mapsto \boldsymbol{v}_{\mathrm{k}}, \quad [1 - r_{\mathrm{a}}]\boldsymbol{v}_{\mathrm{a}} \mapsto \boldsymbol{v}_{\mathrm{a}}, \quad [1 - r_\kappa]v_\kappa \mapsto v_\kappa \tag{51}$$

with $r_{\mathrm{k}}, r_{\mathrm{a}}, r_\kappa \in [0, 1]$ being obvious.

6. Numerical examples

For conceptual simplicity and in order to place emphasis on characteristic properties of the proposed prototype model, we first restrict ourselves to a rate-independent setting in simple shear whereby the effects of degradation and kinematic hardening are discussed separately. Even though the cases of loading and un-/reloading are highlighted within these examples, we further elaborate on cyclic loading in simple shear and thereby additionally account for the rate-dependent case. Finally a finite element setting is discussed, namely the classical example of a rod under torsion whereby all

previously highlighted effects are taken into account, i.e. viscoplasticity, anisotropic degradation, kinematic hardening and proportional hardening.

The following material parameters serve for the subsequent numerical applications: $L \doteq 1.2 \times 10^5$, $G \doteq 8.1 \times 10^4$ (which approximately corresponds to $E = 2.1 \times 10^5$, $\nu = 0.3$), $Y_0 \doteq 5 \times 10^2$, $Y_\infty \doteq 1 \times 10^3$, $K_\infty = 2.5 \times 10^2$, $H_1 \doteq 20$, $H_2 \doteq 1$, $H_3 \doteq 2.5 \times 10^2$ and $D = 10$. Moreover, two different initial (elastic) settings are considered, namely an initially isotropic and an initially anisotropic material. The underlying damage mapping for the first type of material is consequently represented by the identity

$$\boldsymbol{F}_{\mathrm{a}}\,|_{t_0} \doteq \delta_{ij}\boldsymbol{e}_i \otimes \boldsymbol{e}_j, \quad i,j = 1,2,3$$

with δ_{ij} denoting the Kronecker delta and $\{\boldsymbol{e}_i\}$ being a space-attached Cartesian frame.

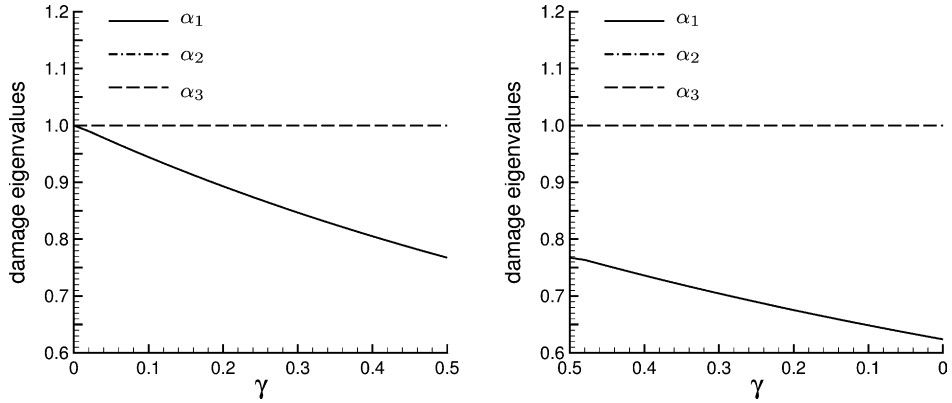

Fig. 2. Simple shear, initially isotropic material (elastoplasticity): eigenvalues $\alpha_{1,2,3}$ of the damage metric $\widehat{\boldsymbol{A}}^{-1}$ for $\gamma \in [0 \to 0.5, 0.5 \to 0]$ and $r_\kappa = r_{\mathrm{k}} = 1$, $r_{\mathrm{a}} = 0$ (no hardening but anisotropic damage).

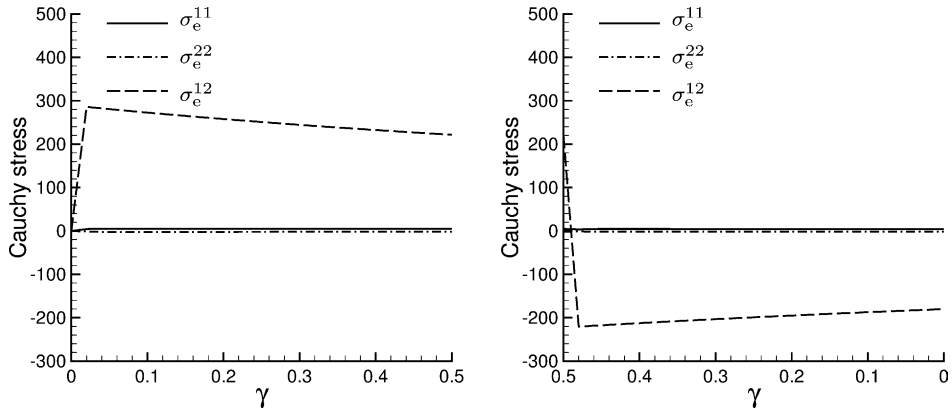

Fig. 3. Simple shear, initially isotropic material (elastoplasticity): Cauchy stress $\boldsymbol{\sigma}_{\mathrm{e}}$ for $\gamma \in [0 \to 0.5, 0.5 \to 0]$ and $r_\kappa = r_{\mathrm{k}} = 1$, $r_{\mathrm{a}} = 0$ (no hardening but anisotropic damage).

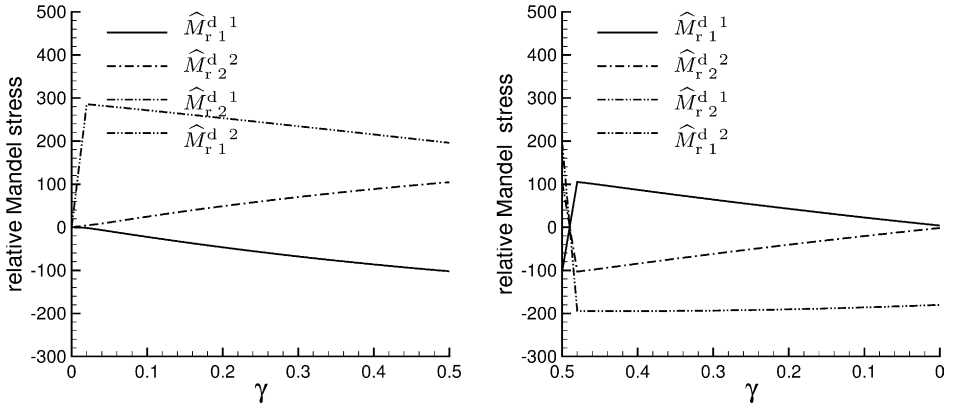

Fig. 4. Simple shear, initially isotropic material (elastoplasticity): relative Mandel stress $\widehat{\boldsymbol{M}}^{\mathrm{d}}_{\mathrm{r}}$ for $\gamma \in [0 \to 0.5, 0.5 \to 0]$ and $r_\kappa = r_{\mathrm{k}} = 1$, $r_{\mathrm{a}} = 0$ (no hardening but anisotropic damage).

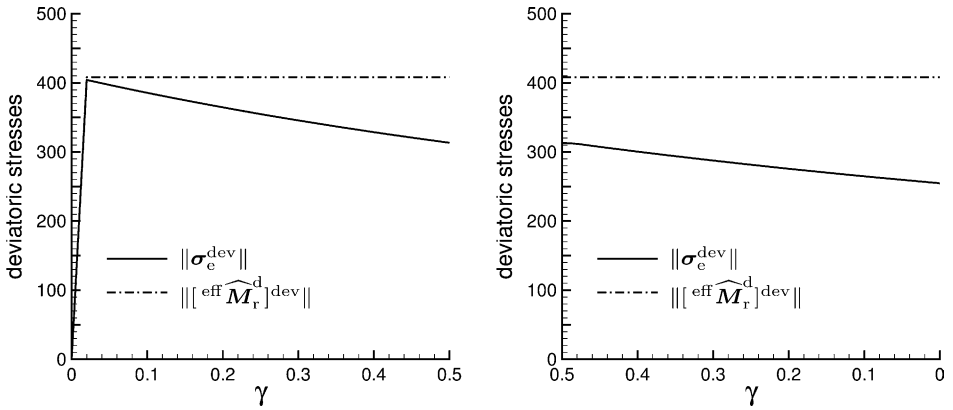

Fig. 5. Simple shear, initially isotropic material (elastoplasticity): norm of the deviatoric stress fields $\boldsymbol{\sigma}^{\mathrm{dev}}_{\mathrm{e}}$ and $[{}^{\mathrm{eff}}\widehat{\boldsymbol{M}}^{\mathrm{d}}_{\mathrm{r}}]^{\mathrm{dev}}$ for $\gamma \in [0 \to 0.5, 0.5 \to 0]$ and $r_\kappa = r_{\mathrm{k}} = 1$, $r_{\mathrm{a}} = 0$ (no hardening but anisotropic damage).

The second material-type, i.e. the initially anisotropic setting, is defined via

$$\boldsymbol{F}_{\mathrm{a}}\,|_{t_0} \doteq 1.0315\boldsymbol{e}_1 \otimes \boldsymbol{e}_1 + 0.9846\boldsymbol{e}_2 \otimes \boldsymbol{e}_2 + 0.9846\boldsymbol{e}_3 \otimes \boldsymbol{e}_3 + 0.0938\boldsymbol{e}_1 \otimes \boldsymbol{e}_2 + 0.0469\boldsymbol{e}_1 \otimes \boldsymbol{e}_3$$

which results via the spectral decomposition theorem, $\widehat{\boldsymbol{A}}^{-1}\,|_{t_0} = \sum_{i=1}^{3} \alpha_{0\,i}\, \widehat{\boldsymbol{V}}_{0\,i} \otimes \widehat{\boldsymbol{V}}_{0\,i}$ with $\|\widehat{\boldsymbol{V}}_{0\,i}\|_{\widehat{\boldsymbol{G}}} = 1$, in

$$\alpha_{0\,1} = 0.9063,\ \widehat{\boldsymbol{V}}_{0\,1} = -0.5220\boldsymbol{e}_1 + 0.7629\boldsymbol{e}_2 + 0.3815\boldsymbol{e}_3,$$
$$\alpha_{0\,2} = 0.9695,\ \widehat{\boldsymbol{V}}_{0\,2} = -0.4472\boldsymbol{e}_2 + 0.8944\boldsymbol{e}_3,$$
$$\alpha_{0\,3} = 1.1381,\ \widehat{\boldsymbol{V}}_{0\,3} = 0.8530\boldsymbol{e}_1 + 0.4669\boldsymbol{e}_2 + 0.2334\boldsymbol{e}_3$$

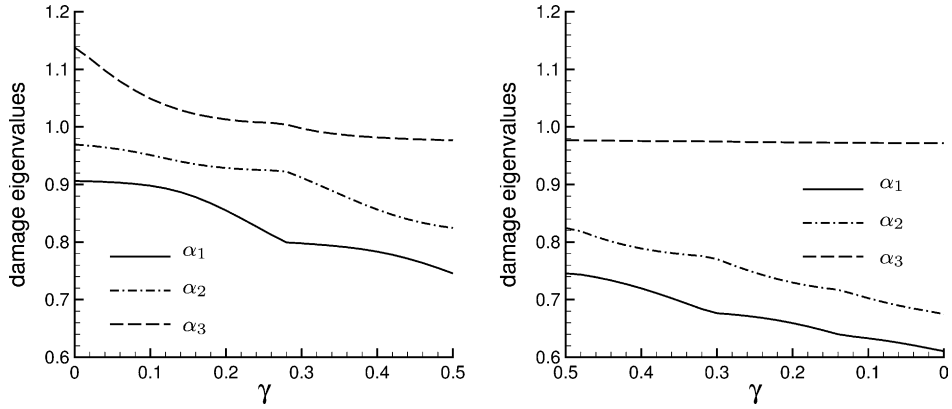

Fig. 6. Simple shear, initially anisotropic material (elastoplasticity): eigenvalues $\alpha_{1,2,3}$ of the damage metric $\widehat{\boldsymbol{A}}^{-1}$ for $\gamma \in [0 \to 0.5, 0.5 \to 0]$ and $r_\kappa = r_\mathrm{k} = 1$, $r_\mathrm{a} = 0$ (no hardening but anisotropic damage).

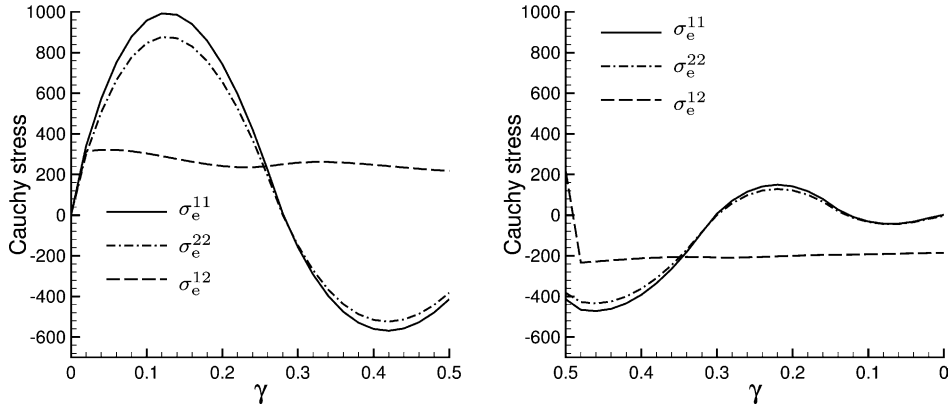

Fig. 7. Simple shear, initially anisotropic material (elastoplasticity): Cauchy stress $\boldsymbol{\sigma}_\mathrm{e}$ for $\gamma \in [0 \to 0.5, 0.5 \to 0]$ and $r_\kappa = r_\mathrm{k} = 1$, $r_\mathrm{a} = 0$ (no hardening but anisotropic damage).

with $\prod_{i=1}^{3} \alpha_{0\,i} = 1$. Please note that the restriction to initially unimodular mappings $\boldsymbol{F}_\mathrm{a}\,|_{t_0}$ is by no means necessary; however, the comparison of the initially isotropic and anisotropic setting would be somehow misleading if $\det(\boldsymbol{F}_\mathrm{a}|_{t_0})$ takes different values for both cases.

In order to visualize that two second order tensors do not commute, we introduce a scalar-valued field, called anisotropy measure, which takes in terms of, e.g., strain and stress the following format:

$$\delta(\widehat{\boldsymbol{E}}_\mathrm{e} \cdot \widehat{\boldsymbol{S}}_\mathrm{e}) = \frac{\|[\widehat{\boldsymbol{E}}_\mathrm{e} \cdot \widehat{\boldsymbol{S}}_\mathrm{e}] - [\widehat{\boldsymbol{E}}_\mathrm{e} \cdot \widehat{\boldsymbol{S}}_\mathrm{e}]^\mathrm{t}\|}{\|\widehat{\boldsymbol{E}}_\mathrm{e} \cdot \widehat{\boldsymbol{S}}_\mathrm{e}\|}.$$

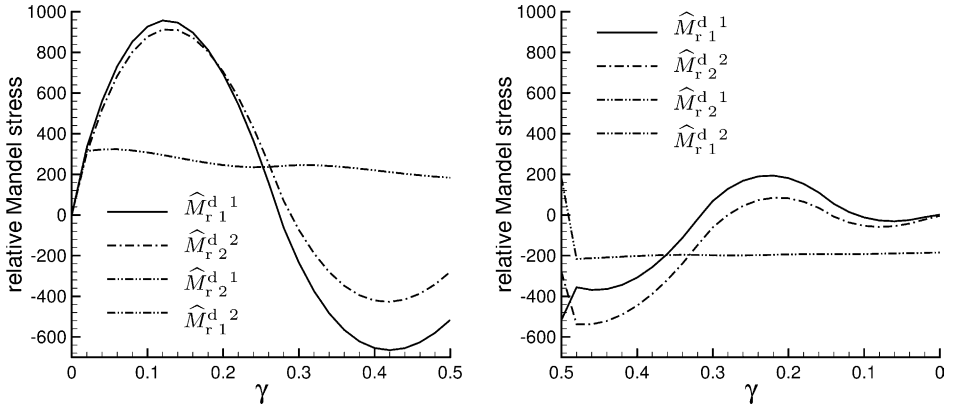

Fig. 8. Simple shear, initially anisotropic material (elastoplasticity): relative Mandel stress $\widehat{\boldsymbol{M}}^{\mathrm{d}}_{\mathrm{r}}$ for $\gamma \in [0 \to 0.5, 0.5 \to 0]$ and $r_\kappa = r_{\mathrm{k}} = 1$, $r_{\mathrm{a}} = 0$ (no hardening but anisotropic damage).

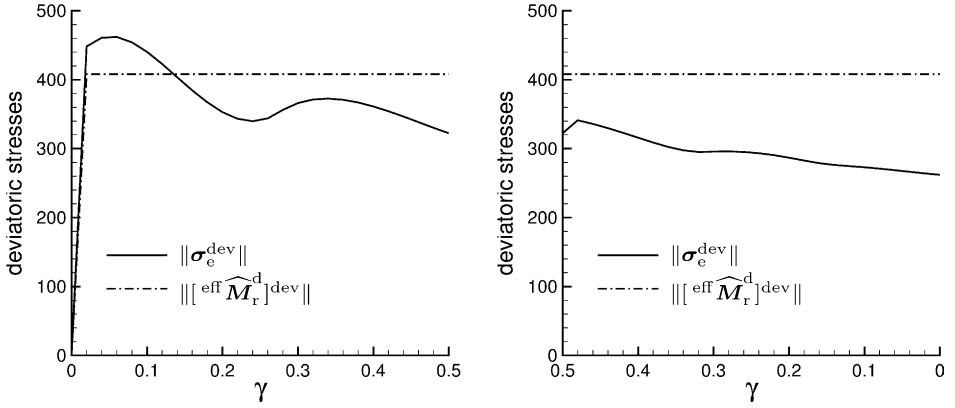

Fig. 9. Simple shear, initially anisotropic material (elastoplasticity): norm of the deviatoric stress fields $\boldsymbol{\sigma}^{\mathrm{dev}}_{\mathrm{e}}$ and $[{}^{\mathrm{eff}}\widehat{\boldsymbol{M}}^{\mathrm{d}}_{\mathrm{r}}]^{\mathrm{dev}}$ for $\gamma \in [0 \to 0.5, 0.5 \to 0]$ and $r_\kappa = r_{\mathrm{k}} = 1$, $r_{\mathrm{a}} = 0$ (no hardening but anisotropic damage).

6.1. Simple shear

The considered homogeneous deformation in simple shear is determined by the deformation gradient $\boldsymbol{F} \doteq \delta_{ij}\,\boldsymbol{e}_i \otimes \boldsymbol{e}_j + \gamma\ \boldsymbol{e}_1 \otimes \boldsymbol{e}_2$. The subsequently applied loading and un-/reloading path is defined by first increasing the shear number from zero to $\frac{1}{2}$, $\gamma \in [0 \to 0.5]$, and second decreasing the shear number back to zero, $\gamma \in [0 \to 0.5, 0.5 \to 0]$. For the cyclic loading history (solely one cycle) the same deformation path is additionally attached, but with revers shear direction.

6.1.1. Elastoplasticity coupled to continuum damage without hardening

The modeling of elastoplasticity with degradation but without hardening is performed via $r_\kappa = r_{\mathrm{k}} = 1$, $r_{\mathrm{a}} = 0$. Fig. 2 highlights the monotonic decrease of the

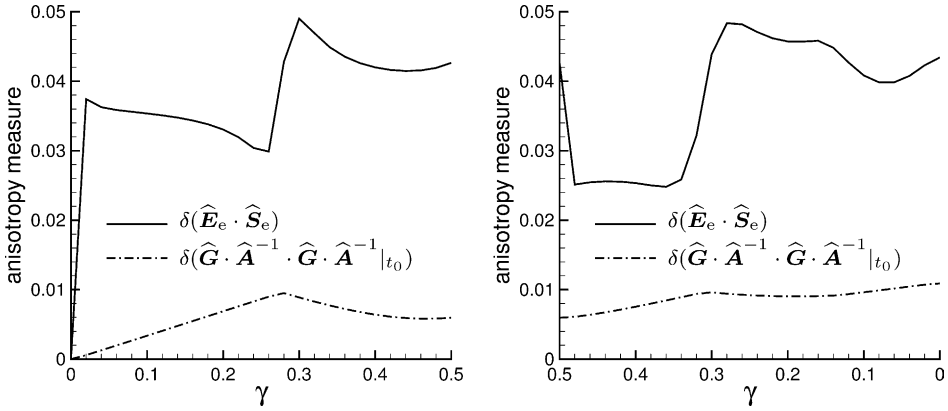

Fig. 10. Simple shear, initially anisotropic material (elastoplasticity): anisotropy measures $\delta(\widehat{\boldsymbol{E}}_{\mathrm{e}} \cdot \widehat{\boldsymbol{S}}_{\mathrm{e}})$, $\delta(\widehat{\boldsymbol{G}} \cdot \widehat{\boldsymbol{A}}^{-1} \cdot \widehat{\boldsymbol{G}} \cdot \widehat{\boldsymbol{A}}^{-1}|_{t_0})$ for $\gamma \in [0 \to 0.5, 0.5 \to 0]$ and $r_\kappa = r_{\mathrm{k}} = 1$, $r_{\mathrm{a}} = 0$ (no hardening but anisotropic damage).

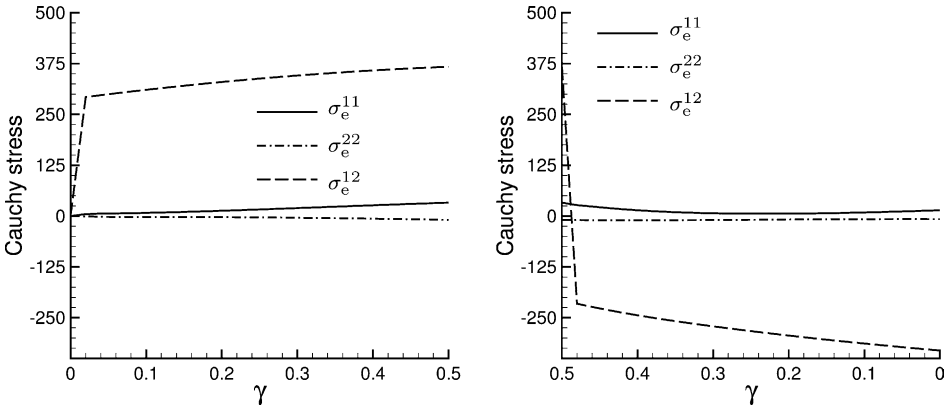

Fig. 11. Simple shear, initially isotropic material (elastoplasticity): Cauchy stress $\boldsymbol{\sigma}_{\mathrm{e}}$ for $\gamma \in [0 \to 0.5, 0.5 \to 0]$ and $r_\kappa = r_{\mathrm{a}} = 1$, $r_{\mathrm{k}} = 0$ (no proportional hardening and damage but kinematic hardening).

eigenvalues of the damage metric for the initially isotropic setting. Apparently, the considered shear deformation results in a high degree of damage evolution. Single components of the Cauchy stress and the relative (or rather elastic) Mandel stress are monitored in Figs. 3 and 4. Furthermore, the deviatoric norms of the Cauchy stress and the effective relative Mandel stress underline on the one hand the degradation of the material and on the other the fact that no proportional hardening is taken into account, see Fig. 5. The rather small elastic range is clearly displayed in Figs. 3–5.

Next, the initially anisotropic material is discussed. Figs. 6–9 monitor the damage metric and stress fields of interest in analogy to the previous setting. The damage eigenvalues degrade similar to the isotropic case but follow distinctive evolutions, see

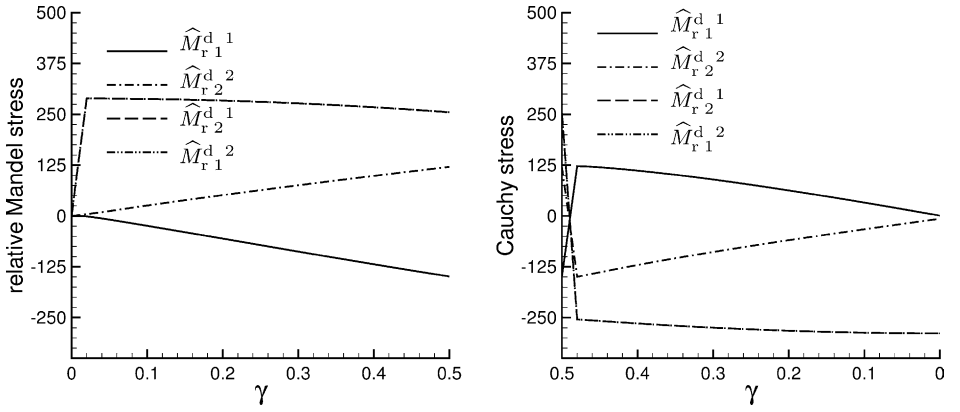

Fig. 12. Simple shear, initially isotropic material (elastoplasticity): relative Mandel stress $\widehat{\boldsymbol{M}}_{\mathrm{r}}^{\mathrm{d}}$ for $\gamma \in [0 \to 0.5, 0.5 \to 0]$ and $r_\kappa = r_{\mathrm{a}} = 1$, $r_{\mathrm{k}} = 0$ (no proportional hardening and damage but kinematic hardening).

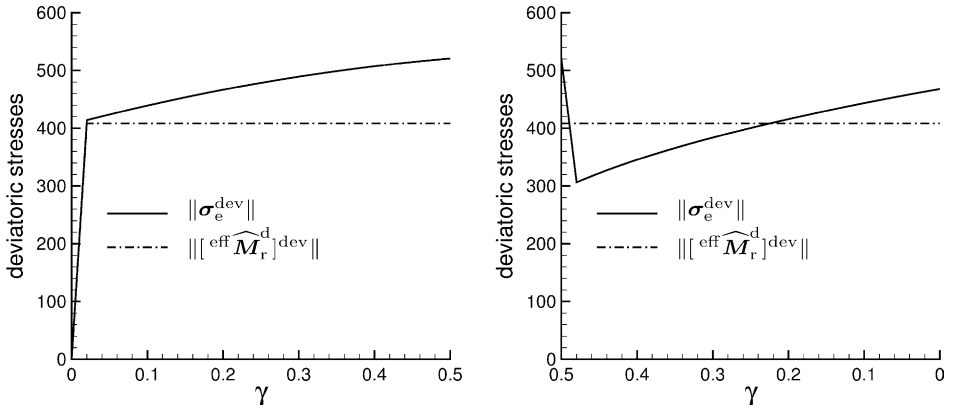

Fig. 13. Simple shear, initially isotropic material (elastoplasticity): norm of the deviatoric stress fields $\boldsymbol{\sigma}_{\mathrm{e}}^{\mathrm{dev}}$ and $[{}^{\mathrm{eff}}\widehat{\boldsymbol{M}}_{\mathrm{r}}^{\mathrm{d}}]^{\mathrm{dev}}$ for $\gamma \in [0 \to 0.5, 0.5 \to 0]$ and $r_\kappa = r_{\mathrm{a}} = 1$, $r_{\mathrm{k}} = 0$ (no proportional hardening and damage but kinematic hardening).

Fig. 6. Both the Cauchy stress and the relative Mandel stress possess completely different properties compared to the previous setting, Figs. 7 and 8 whereby the cyclic response apparently stems from the incorporated anisotropy, the deviatoric stress norms however monitor once more the perfectly plastic behavior, Fig. 9. For the initially anisotropic setting we place additional emphasis on two anisotropy measures, see Fig. 10. It is clearly seen that the overall response is anisotropic and, furthermore, that the principal directions of the damage metric evolve during the considered deformation process.

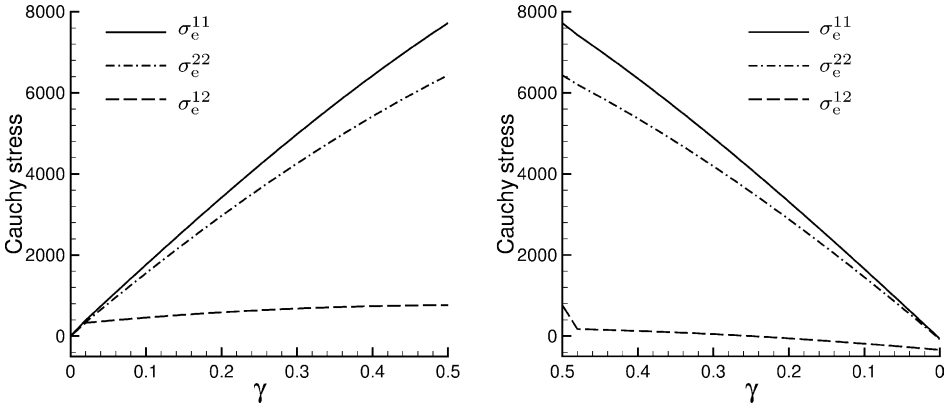

Fig. 14. Simple shear, initially anisotropic material (elastoplasticity): Cauchy stress $\boldsymbol{\sigma}_e$ for $\gamma \in [0 \to 0.5, 0.5 \to 0]$ and $r_\kappa = r_a = 1$, $r_k = 0$ (no proportional hardening and damage but kinematic hardening).

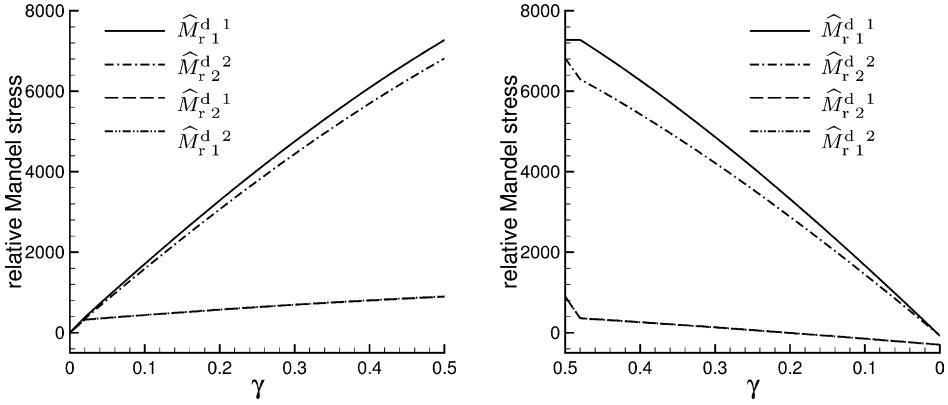

Fig. 15. Simple shear, initially anisotropic material (elastoplasticity): relative Mandel stress $\widehat{\boldsymbol{M}}_r^d$ for $\gamma \in [0 \to 0.5, 0.5 \to 0]$ and $r_\kappa = r_a = 1$, $r_k = 0$ (no proportional hardening and damage but kinematic hardening).

6.1.2. Elastoplasticity with kinematic hardening but without degradation

Apparently, elastoplasticity with solely kinematic hardening but without degradation is represented via $r_\kappa = r_a = 1$, $r_k = 0$. The initially isotropic setting clearly monitors a typical behavior as expected for kinematic hardening, see the visualization of the Cauchy stress, the relative Mandel stress and the deviatoric norms of these stress fields in Figs. 11–13. We observe in particular the saturation-type effect and that the admissible domain is dragged along as well as that proportional hardening is not incorporated.

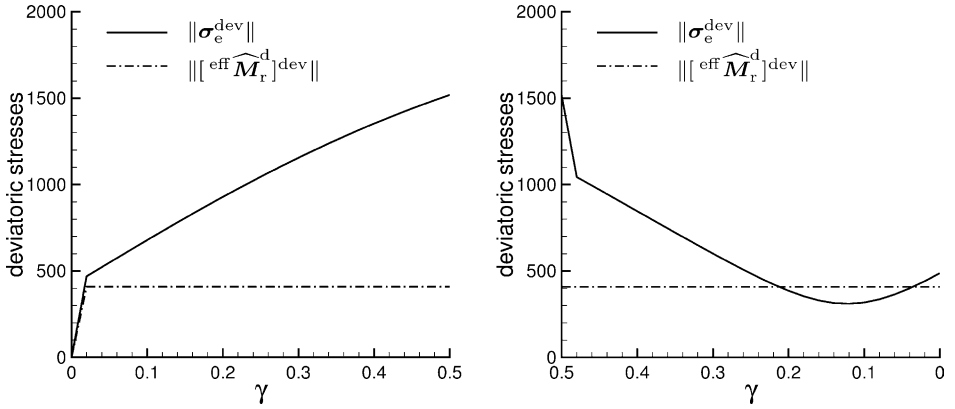

Fig. 16. Simple shear, initially anisotropic material (elastoplasticity): norm of the deviatoric stress fields $\boldsymbol{\sigma}_{\mathrm{e}}^{\mathrm{dev}}$ and $[{}^{\mathrm{eff}}\widehat{\boldsymbol{M}}_{\mathrm{r}}^{\mathrm{d}}]^{\mathrm{dev}}$ for $\gamma \in [0 \to 0.5, 0.5 \to 0]$ and $r_\kappa = r_{\mathrm{a}} = 1$, $r_{\mathrm{k}} = 0$ (no proportional hardening and damage but kinematic hardening).

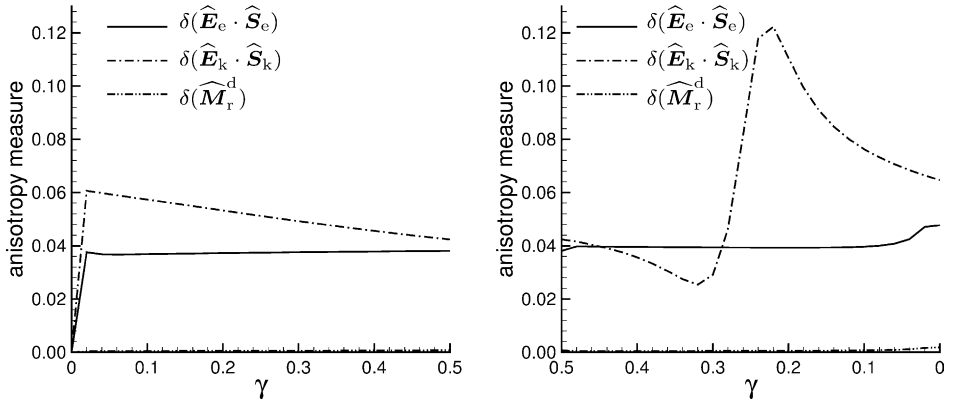

Fig. 17. Simple shear, initially anisotropic material (elastoplasticity): anisotropy measures $\delta(\widehat{\boldsymbol{E}}_{\mathrm{e}} \cdot \widehat{\boldsymbol{S}}_{\mathrm{e}})$, $\delta(\widehat{\boldsymbol{E}}_{\mathrm{k}} \cdot \widehat{\boldsymbol{S}}_{\mathrm{k}})$, $\delta(\widehat{\boldsymbol{M}}_{\mathrm{r}}^{\mathrm{d}})$ for $\gamma \in [0 \to 0.5, 0.5 \to 0]$ and $r_\kappa = r_{\mathrm{a}} = 1$, $r_{\mathrm{k}} = 0$ (no proportional hardening and damage but kinematic hardening).

Figs. 14–17 highlight the behavior of the initially anisotropic material. The material response turns out be completely different compared to the monitored Cauchy stress and the relative Mandel stress for the isotropic setting in Figs. 11–13. The fact that proportional hardening is not activated is clearly visualized in Fig. 16. Due to the overall anisotropy of the material and the non-constant principal strain directions in simple shear we compute several non-vanishing anisotropy measures. These scalar-valued fields that represent the non-commutativity of the considered tensorial quantities are monitored in Fig. 17.

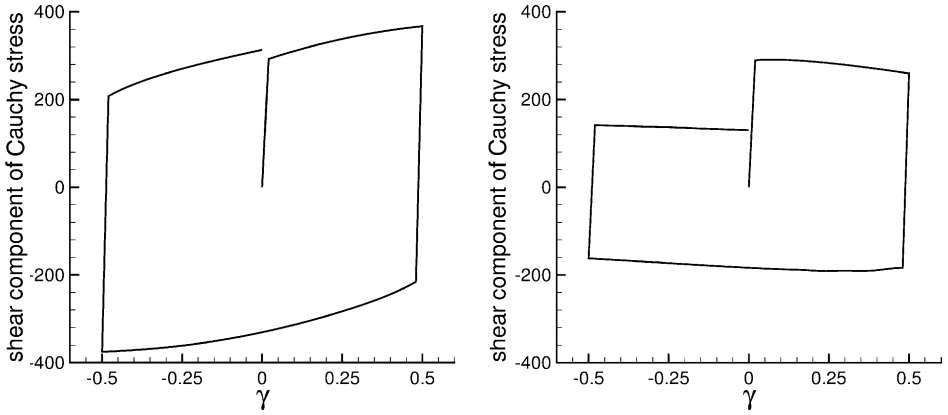

Fig. 18. Simple shear, initially isotropic material (elastoplasticity): shear component of the Cauchy stress σ_e^{12} for $\gamma \in [0 \to 0.5, 0.5 \to -0.5, -0.5 \to 0]$ and $r_\kappa = r_a = 1$, $r_k = 0$ (no proportional hardening and damage but kinematic hardening; left) and $r_\kappa = 1$, $r_k = r_a = 0$ (no proportional hardening but kinematic hardening and anisotropic damage; right).

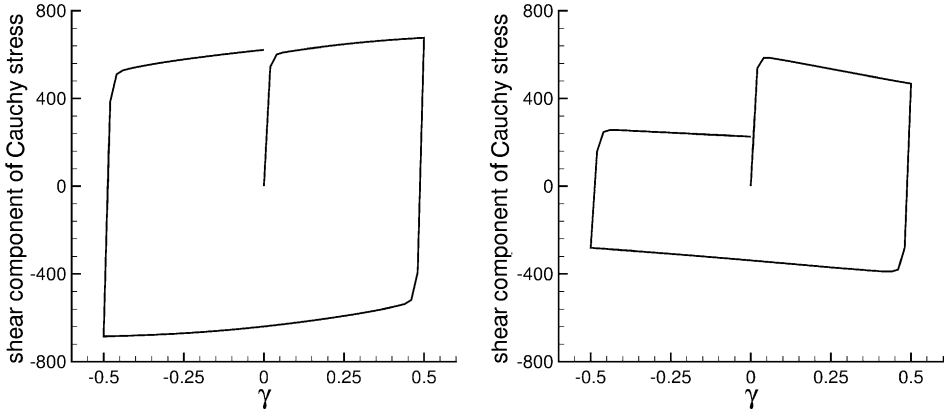

Fig. 19. Simple shear, initially isotropic material (elastoviscoplasticity): shear component of the Cauchy stress σ_e^{12} for $\gamma \in [0 \to 0.5, 0.5 \to -0.5, -0.5 \to 0]$ and $r_\kappa = r_a = 1$, $r_k = 0$ (no proportional hardening and damage but kinematic hardening; left) and $r_\kappa = 1$, $r_k = r_a = 0$ (no proportional hardening but kinematic hardening and anisotropic damage; right).

6.1.3. Cyclic loading

Next, a representative cyclic loading path is considered whereby for the sake of clarity solely one cycle is taken into account. The subsequent graphs highlight the shear component of the (elastic) Cauchy stress, σ_e^{12}, with respect to a space-attached Cartesian frame. For the initially isotropic setting, Fig. 18 visualizes the response for kinematic hardening without and with degradation. We observe for the first case that the nonlinear saturation-type effect of kinematic hardening is captured by the applied prototype model. Both effects, the typical influence of the back-stress as well as

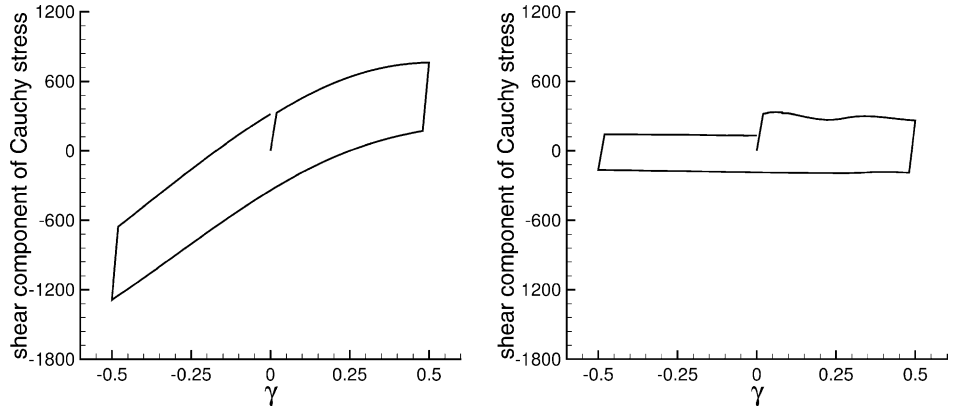

Fig. 20. Simple shear, initially anisotropic material (elastoplasticity): shear component of the Cauchy stress σ_e^{12} for $\gamma \in [0 \to 0.5, 0.5 \to -0.5, -0.5 \to 0]$ and $r_\kappa = r_a = 1$, $r_k = 0$ (no proportional hardening and damage but kinematic hardening; left) and $r_\kappa = 1$, $r_a = r_k = 0$ (no proportional hardening but kinematic hardening and anisotropic damage; right).

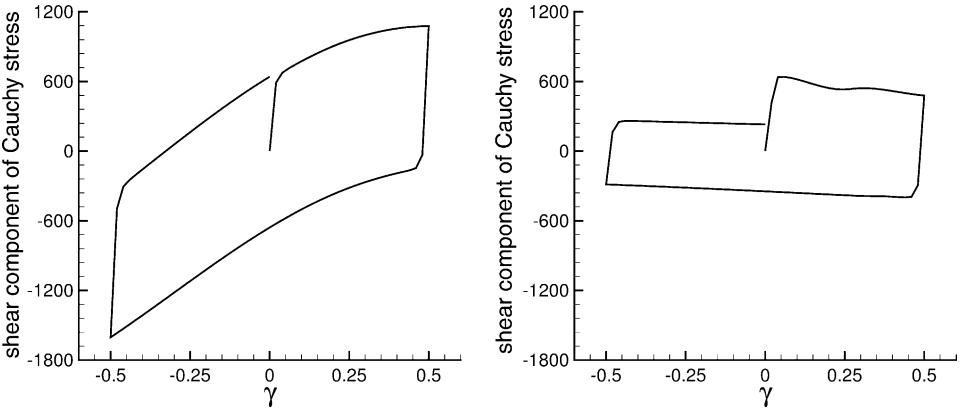

Fig. 21. Simple shear, initially anisotropic material (elastoviscoplasticity): shear component of the Cauchy stress σ_e^{12} for $\gamma \in [0 \to 0.5, 0.5 \to -0.5, -0.5 \to 0]$ and $r_\kappa = r_a = 1$, $r_a = 0$ (no proportional hardening and damage but kinematic hardening; left) and $r_\kappa = 1$, $r_a = r_k = 0$ (no proportional hardening but kinematic hardening and anisotropic damage; right).

the decrease of the Cauchy stress due to damage evolution are clearly monitored. On top of that, the computations displayed in Fig. 19 additionally account for viscoplastic behavior. Thereby the time interval of the loading path is set to $\mathbb{T} = 100$, which defines the time increments Δt, the relaxation time has been chosen as $t_{rel} = 100$ and in view of the power-type law we assumed $N = 2$.

Finally, Figs. 20 and 21 highlight similar results for the initially anisotropic material. It is thereby obvious that due to the incorporated anisotropy the shear stress

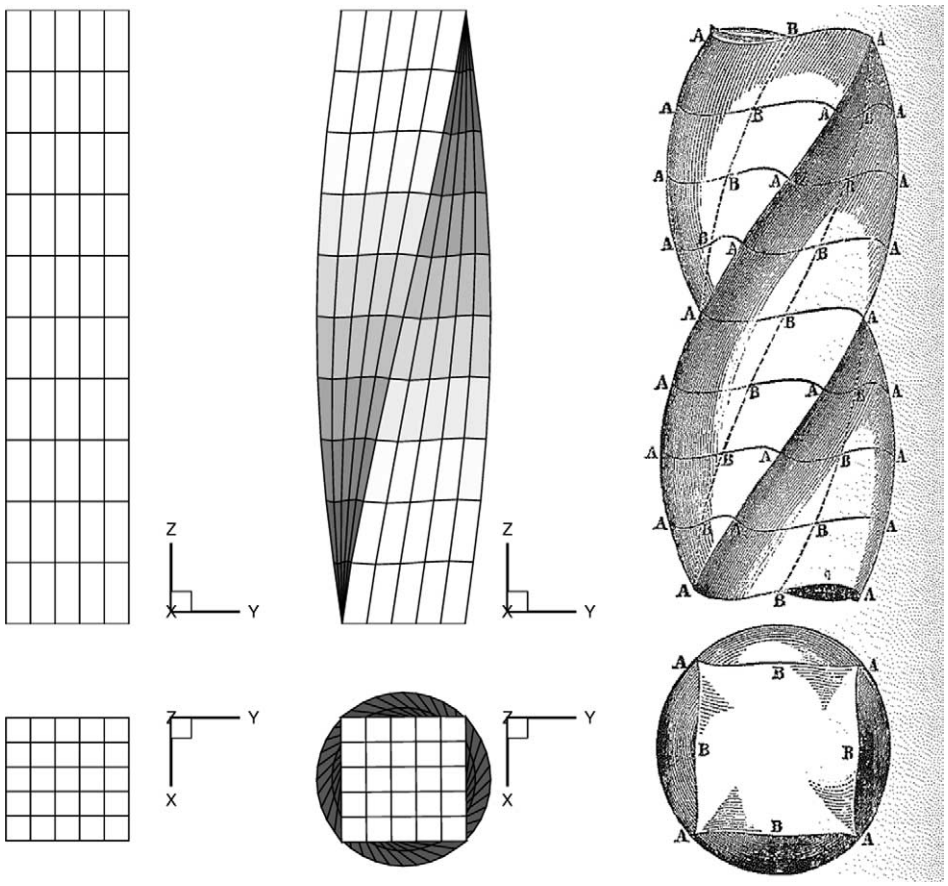

Fig. 22. Torsion of a rod, initially anisotropic material: discretization (left), deformed mesh for $\varphi \in [0 \rightarrow \frac{\pi}{2}]$ (middle) and drawing by St. Venant (right), taken from Fung and Tong (2001).

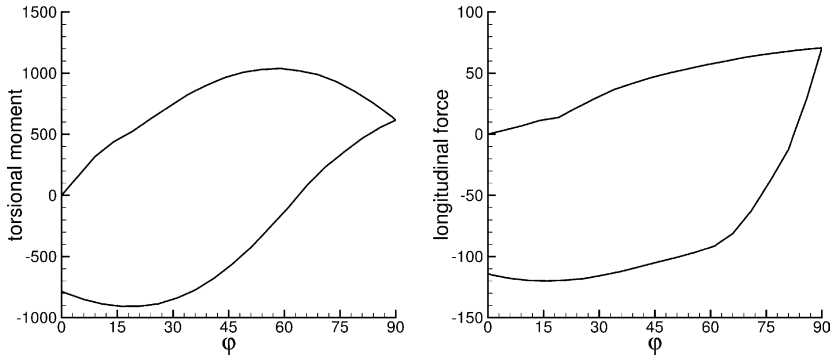

Fig. 23. Torsion of a rod, initially anisotropic material (elastoviscoplasticity): torsional moment (left), longitudinal force (right) for $\varphi \in [0 \rightarrow \frac{\pi}{2}, \frac{\pi}{2} \rightarrow 0]$ and $r_\kappa = 0.75$, $r_\mathrm{k} = 0.25$, $r_\mathrm{a} = 0$ (proportional and non-linear saturation-type kinematic hardening and anisotropic damage).

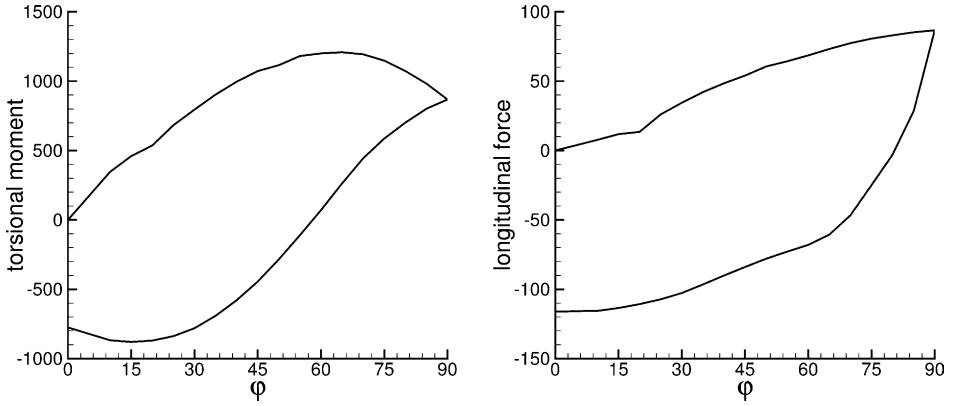

Fig. 24. Torsion of a rod, initially anisotropic material (elastoviscoplasticity): torsional moment (left), longitudinal force (right) for $\varphi \in [0 \to \frac{\pi}{2}, \frac{\pi}{2} \to 0]$ and $r_\kappa = 0.75$, $r_\mathrm{k} = 0.25$, $r_\mathrm{a} = 0$ (proportional and linear kinematic hardening and anisotropic damage).

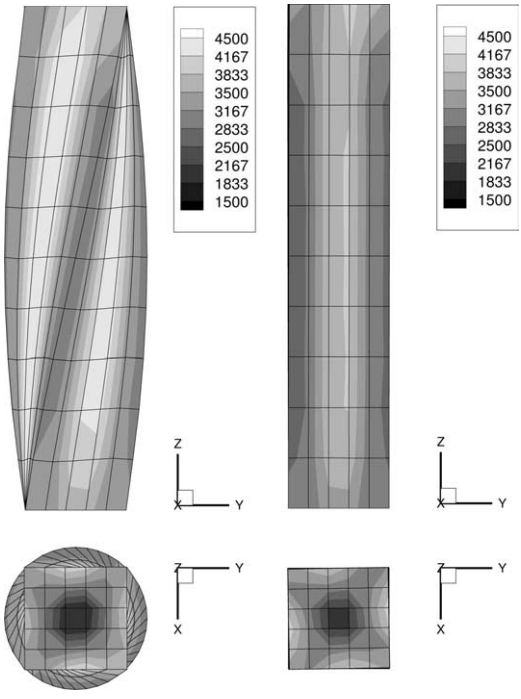

Fig. 25. Torsion of a rod, initially anisotropic material (elastoviscoplasticity): norm of $\boldsymbol{\sigma}_\mathrm{e}^\mathrm{dev}$ for $\varphi \in [0 \to \frac{\pi}{2}]$ (left), $\varphi \in [0 \to \frac{\pi}{2}, \frac{\pi}{2} \to 0]$ (right) and $r_\kappa = 0.75$, $r_\mathrm{k} = 0.25$, $r_\mathrm{a} = 0$ (proportional and kinematic hardening and anisotropic damage).

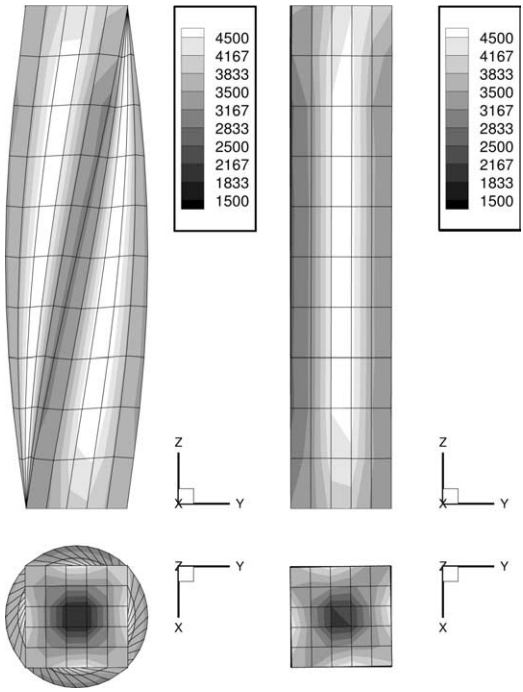

Fig. 26. Torsion of a rod, initially anisotropic material (elastoviscoplasticity): norm of $[^{\mathrm{eff}}\widehat{\boldsymbol{M}}_{\mathrm{r}}^{\mathrm{d}}]^{\mathrm{dev}}$ for $\varphi \in [0 \to \frac{\pi}{2}]$ (left), $\varphi \in [0 \to \frac{\pi}{2}, \frac{\pi}{2} \to 0]$ (right) and $r_\kappa = 0.75$, $r_{\mathrm{k}} = 0.25$, $r_{\mathrm{a}} = 0$ (proportional and kinematic hardening and anisotropic damage).

components σ_{e}^{23} and σ_{e}^{13} do not vanish. However, in analogy to the previous setting we restrict ourselves to the visualization of the response on σ_{e}^{12}.

6.2. Torsion of a rod

Completing the numerical examples, we lastly focus on a finite element setting. The considered boundary value problem is a typical torsion problem of a rod as commonly elaborated in experimental and numerical investigation on the plastic behavior of metallic materials. To be specific, the cross-section at the bottom of the rod is completely clamped while the cross-section at the top of the rod is rotated which allows to be measured in terms of an angle φ. Longitudinal displacements of the top cross-section are nevertheless prevented and we therefore observe a longitudinal force in addition to the torsional moment. Fig. 22 gives a graphical representation of the considered specimen. The geometry of the square rod is chosen as $1 \times 1 \times 5$ and the discretization is performed by $5 \times 5 \times 10$ enhanced eight node bricks (Q1E9) as advocated by Simo and Armero (1992). No emphasis is placed on the finite element implementation itself in this work but the reader is rather referred

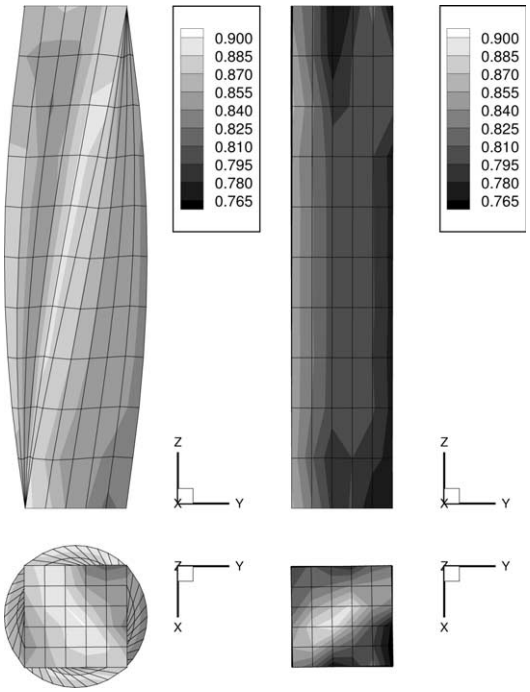

Fig. 27. Torsion of a rod, initially anisotropic material (elastoviscoplasticity): smallest damage eigenvalue α_1 for $\varphi \in [0 \to \frac{\pi}{2}]$ (left), $\varphi \in [0 \to \frac{\pi}{2}, \frac{\pi}{2} \to 0]$ (right) and $r_\kappa = 0.75$, $r_\mathrm{k} = 0.25$, $r_\mathrm{a} = 0$ (proportional and kinematic hardening and anisotropic damage).

to the monographs by, e.g., Oden (1972) or Belytschko et al. (2000) and references cited therein.

In the sequel we account for viscoplasticity, initial anisotropy, anisotropic degradation, kinematic and proportional hardening; $\mathrm{r}_\kappa = 0.75$, $\mathrm{r}_\mathrm{k} = 0.25$, $r_\mathrm{a} = 0$. Thereby, the rotation or rather torsion angle φ is first increased from zero to $\frac{\pi}{2}$ and then boiled down to zero such that loading and un-/reloading is modeled; $\varphi \in [0 \to \frac{\pi}{2}, \frac{\pi}{2} \to 0]$. Rate-dependency is characterized via the parameters $N = 1$, $t_\mathrm{rel} = 1000$ and the loading path from zero up to $\varphi = \frac{\pi}{2}$ is related to the time interval $\mathbb{T} = 9$ (the un-/reloading path is related to the same time interval, i.e $\varphi \in [0 \to \frac{\pi}{2}, \frac{\pi}{2} \to 0]$ corresponds to $\mathbb{T} = 18$). Fig. 23 displays load/displacement curves for the loading and un-/reloading path. We observe in particular that the torsional moment monitors the overall softening behavior for loading and even for un-/reloading. Due to the chosen boundary conditions the longitudinal force shows similar characteristics; at least at the end of the considered un-/reloading path we observe a slight softening behavior. For comparison reasons, we additionally highlight similar load/displacement curves for the, say, linear kinematic hardening model in Fig. 24. These computations, which neglect the extension given in Eq. (50), show higher peak values for the maximum torsional moment as well as for the maximum longitudinal

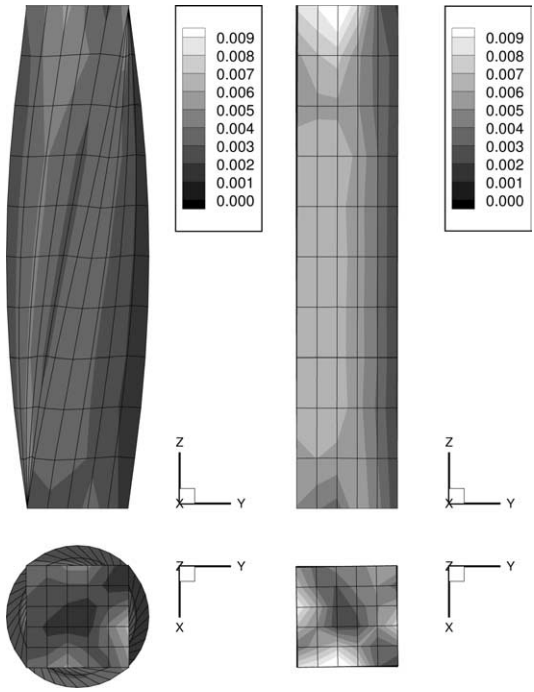

Fig. 28. Torsion of a rod, initially anisotropic material (elastoviscoplasticity): anisotropy measure $\delta(\widehat{\boldsymbol{G}} \cdot \widehat{\boldsymbol{A}}^{-1} \cdot \widehat{\boldsymbol{G}} \cdot \widehat{\boldsymbol{A}}^{-1}|_{t_0})$ for $\varphi \in [0 \to \frac{\pi}{2}]$ (left), $\varphi \in [0 \to \frac{\pi}{2}, \frac{\pi}{2} \to 0]$ (right) and $r_\kappa = 0.75$, $r_\mathrm{k} = 0.25$, $r_\mathrm{a} = 0$ (proportional and kinematic hardening and anisotropic damage).

force. This shift-effect underlines the influence of the non-linear saturation-type kinematic hardening model (the subsequent figures are based on the nonlinear saturation-type model).

Since an initially anisotropic setting is considered, the response of the specimen is throughout non-symmetric. This property is clearly monitored by the deviatoric norm of the (elastic) Cauchy stress and the effective relative Mandel stress, see Figs. 25 and 26 where the loading and and un-/reloading response is highlighted.

The smallest damage eigenvalue, which in fact characterizes the degree of damage, is visualized in Fig. 27. Note that the state of degradation is quite advanced and still increases for the un-/reloading path. Since the principal direction of the damage metric do not remain constant during the deformation process we obtain a non-vanishing anisotropy measure with respect to the actual and initial damage metric which is plotted in Fig. 28.

Finally, the visualization of the corresponding anisotropy measures for the elastic and kinematic hardening contributions are highlighted in Figs. 29 and 30. These plots underline that the related Mandel-type stress tensor are throughout non-symmetric since the underlying related strain and stress fields do not commute.

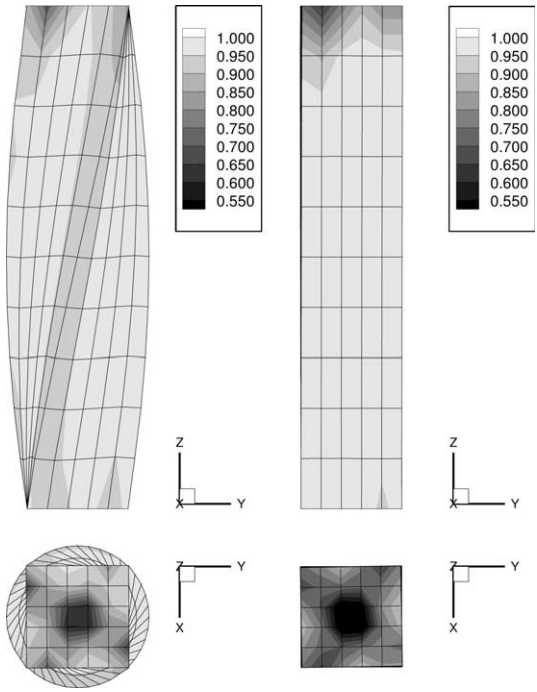

Fig. 29. Torsion of a rod, initially anisotropic material (elastoviscoplasticity): anisotropy measure $\delta(\widehat{\boldsymbol{E}}_{\mathrm{e}} \cdot \widehat{\boldsymbol{S}}_{\mathrm{e}})$ for $\varphi \in [0 \to \frac{\pi}{2}]$ (left), $\varphi \in [0 \to \frac{\pi}{2}, \frac{\pi}{2} \to 0]$ (right) and $r_\kappa = 0.75$, $r_{\mathrm{k}} = 0.25$, $r_{\mathrm{a}} = 0$ (proportional and kinematic hardening and anisotropic damage).

7. Summary

The main goal of this contribution was the development of a formulation of finite anisotropic inelasticity. We considered in particular a viscoplastic setting that accounted for anisotropic degradation and for kinematic as well as proportional hardening. As a key idea, an isotropic fictitious or rather effective configuration has been introduced which is related to the intermediate configuration of multiplicative elastoplasticity via a fictitious or rather damage tangent map. Practically speaking, the covariance principle serves as a basic tool to develop the proposed finite strain setting by assuming the free Helmholtz energy to remain invariant under the action of this mapping. Conceptually speaking we dealt with an Euclidian space with respect to a non-constant metric that allowed to model transversal and orthotropic material symmetry if this damage metric possessed non-spherical properties. In analogy to the damage or rather anisotropy mapping, another tangent has been introduced that served as an internal variable to define a Mandel-type back-stress tensor and therefore allowed to incorporate kinematic hardening.

Straightforward application of the framework of non-standard dissipative materials resulted in appropriate evolution equations. While a generally non-symmetric effective relative Mandel stress tensor has been employed into the yield function, the

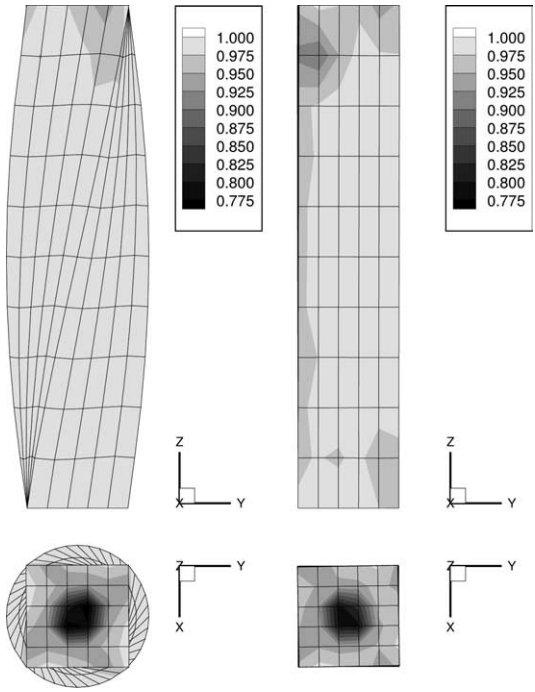

Fig. 30. Torsion of a rod, initially anisotropic material (elastoviscoplasticity): anisotropy measure $\delta(\widehat{\boldsymbol{E}}_{\mathrm{k}} \cdot \widehat{\boldsymbol{S}}_{\mathrm{k}})$ for $\varphi \in [0 \to \frac{\pi}{2}]$ (left), $\varphi \in [0 \to \frac{\pi}{2}, \frac{\pi}{2} \to 0]$ (right) and $r_{\kappa} = 0.75$, $r_{\mathrm{k}} = 0.25$, $r_{\mathrm{a}} = 0$ (proportional and kinematic hardening and anisotropic damage).

Mandel-type damage tensor allowed a generally symmetric representation in the effective configuration. Based on this, exponential integration schemes have been applied to the underlying (inelastic) tangent maps.

The proposed thermodynamically consistent prototype model was based on well-established potentials. However, the kinematic hardening contribution accounted for an additional saturation-type term and in view of the damage evolution a Rankine-type ansatz, as based on a spectral decomposition of the Mandel-type damage stress, has been adopted. The developed formulation therefore accounts for the modeling of different material behavior in tension and compression with respect to the space spanned by the damage stress tensor.

Several numerical examples underlined the applicability of the developed framework. Different properties of the model have been investigated for the rate-independent and rate-dependent case with respect to a homogeneous deformation in simple shear. Both, loading and un-/reloading as well as cyclic loading have been discussed in detail. Finally, a finite element setting was applied to a classical torsion problem and monitored the capability of the proposed formulation to model overall softening behavior, initial anisotropy, kinematic and proportional hardening as well as anisotropic degradation.

References

Antman, S.S., 1995. Nonlinear Problems of Elasticity. In: Applied Mathematical Sciences, vol. 107. Springer, Berlin.

Belytschko, T., Liu, W., Moran, B., 2000. Nonlinear Finite Elements for Continua and Structures. Wiley, New York.

Bertram, A., 1999. An alternative approach to finite plasticity based on material isomorphisms. Int. J. Plasticity 15, 353–374.

Bertram, A., 2003. Finite thermoplasticity based on isomorphisms. Int. J. Plasticity 19, 2027–2050.

Besseling, J., van der Giessen, E., 1994. Mathematical Modelling of Inelastic Deformation. In: Applied Mathematics and Mathematical Computations, vol. 5. Chapman & Hall, London.

Betten, J., 1981. Representation of constitutive equations in creep mechanics of isotropic and anisotropic materials. In: Ponter, A., Hayhurst, D. (Eds.), Creep in Structures. In: IUTAM Symposium Leicester/UK 1980. Springer, Berlin, pp. 179–201.

Bruhns, O., Xiao, H., Meyers, A., 2003. Some basic issues in traditional Eulerian formulations of finite elastoplasticity. Int. J. Plasticity 19, 2007–2026.

Brünig, M., 2003. An anisotropic ductile damage model based on irreversible thermodynamics. Int. J. Plasticity 19, 1679–1714.

Carol, I., Rizzi, E., Willam, K., 2001. On the formulation of anisotropic elastic degradation. Part I: Theory based on a pseudo-logarithmic damage tensor rate, Part II: Generalized pseudo-Rankine model for tensile damage. Int. J. Solids Struct. 38, 491–518, 519–546.

Cleja-Ţigoiu, S., 2000. Nonlinear elasto-plastic deformations of transversely isotropic material and plastic spin. Int. J. Eng. Sci. 38, 737–763.

Dafalias, Y., 1998. Plastic spin: Necessity or redundancy? Int. J. Plasticity 14, 909–931.

Dennis Jr., J., Schnabel, R., 1996. Numerical Methods for Unconstrained Optimization and Nonlinear Equations. In: Classics in Applied Mathematics, vol. 16. SIAM, Philadelphia, PA.

Diegele, E., Jansohn, W., Tsakmakis, C., 2000. Finite deformation plasticity and viscoplasticity laws exhibiting nonlinear hardening rules: Part I: Constitutive theory and numerical integration, Part II: Representative examples. Comput. Mech. 25, 1–12, 13–27.

Ekh, M., Lillbacka, R., Runesson, K. 2003a. A model framework for anisotropic damage coupled to crystal (visco)plasticity. Int. J. Plasticity, (accepted).

Ekh, M., Menzel, A., Runesson, K., Steinmann, P., 2003b. Anisotropic damage with the MCR effect coupled to plasticity. Int. J. Eng. Sci. 41, 1535–1551.

Ekh, M., Runesson, K., 2000. Bifurcation results for plasticity coupled to damage with mcr-effect. Int. J. Solids Struct. 37, 1975–1996.

Ekh, M., Runesson, K., 2001. Modelling and numerical issues in hyperelasto-plasticity with anisotropy. Int. J. Solids Struct. 38, 9461–9478.

Ericksen, J., 1960. Tensor fields. In: Flügge, S. (Ed.), Encyclopedia of Physics, vol. III/1. Springer, Berlin, pp. 794–858.

Eringen, A., 1962. Nonlinear Theory of Continuous Media. Series in Engineering Science. McGraw-Hill, New York.

Eringen, A., 1971. Tensor analysis. In: Eringen, A. (Ed.), Continuum Physics, vol. 1: Mathematics. Academic Press, New York, pp. 1–155.

Fellin, W., Ostermann, A., 2002. Consistent tangent operators for constitutive rate equations. Int. J. Numer. Anal. Meth. Geomech. 26, 1213–1233.

Fung, Y., Tong, P., 2001. Classical and Computational Solid Mechanics. In: Advanced Series in Engineering Science, vol. 1. World Scientific, Singapore.

Govindjee, S., Reese, S., 1997. A presentation and comparison of two large strain deformation visoelasticity models. ASME J. Eng. Mater. Tech. 119, 251–255.

Haupt, P., 2000. Continuum Mechanics and Theory of Materials. Advanced Texts in Physics. Springer, Berlin.

Haupt, P., Kersten, T., 2003. On the modelling of anisotropic material behaviour in viscoplasticity. Int. J. Plasticity 19, 1885–1915.

Häusler, O., Schick, D., Tsakmakis, C., 2004. Description of plastic anisotropy effects at large deformations. Part II: The case of transverse isotropy. Int. J. Plasticity 20, 199–223.
Hill, R., 2000. Plastic anisotropy and the geometry of yield surfaces in stress space. J. Mech. Phys. Solids 48, 1093–1106.
Kattan, P., Voyiadjis, G., 1990. A coupled theory of damage mechanics and finite strain elasto-plasticity – I. Damage and elastic deformations. Int. J. Eng. Sci. 28, 421–435.
Khan, A., Huang, S., 1995. Continuum Theory of Plasticity. Wiley, New York.
Lämmer, H., Tsakmakis, C., 2000. Discussion of coupled elastoplasticity and damage constitutive equations for small and finite deformations. Int. J. Plasticity 16, 495–523.
Leckie, F., Onat, E., 1981. Tensorial nature of damage measuring internal variables. In: Hult, J., Lemaitre, J. (Eds.), Physical Non-Linearities in Structural Analysis. In: IUTAM Symposium Senlis/France 1980. Springer, Berlin, pp. 140–155.
Lemaitre, J., Chaboche, J.-L., 1998. Mechanics of Solid Materials, second ed. Cambridge University Press, Cambridge.
Lodge, A., 1974. Body Tensor Fields in Continuum Mechanics – With Application to Polymer Rheology. Academic Press, New York.
Lu, J., 2003. A covariant condition and related constitutive results in finite plasticity. Z. Angew. Math. Phys. (accepted).
Lu, J., Papadopoulos, P., 2000. A covariant constitutive description of anisotropic non-linear elasticity. Z. Angew. Math. Phys. 51, 204–217.
Lubarda, V., 2002. Elastoplasticity Theory. Mechanical Engineering Series. CRC Press, Boca Raton.
Lubliner, J., 1990. Plasticity Theory. MacMillan Publishing Company.
Marsden, J., Hughes, T., 1994. Mathematical Foundations of Elasticity. Dover.
Maugin, G., 1992. The Thermomechanics of Plasticity and Fracture. Cambridge Texts in Applied Mathematics. Cambridge University Press, Cambridge.
Maugin, G., 1999. The Thermodynamics of Nonlinear Irreversible Behaviors. In: World Scientific Series on Nonlinear Science: Series A, vol. 27. World Scientific, Singapore.
Menzel, A., Carol, I., Steinmann, P. 2003. A framework for (visco)plasticity coupled to anisotropic damage. In: Proceedings of COMPLAS VII, Barcelona.
Menzel, A., Ekh, M., Steinmann, P., Runesson, K., 2002. Anisotropic damage coupled to plasticity: Modelling based on the effective configuration concept. Int. J. Numer. Meth. Eng. 54, 1409–1430.
Menzel, A., Steinmann, P., 2001a. On the comparison of two strategies to formulate orthotropic hyperelasticity. J. Elasticity 62, 171–201.
Menzel, A., Steinmann, P., 2001b. A theoretical and computational setting for anisotropic continuum damage mechanics at large strains. Int. J. Solids Struct. 38, 9505–9523.
Menzel, A., Steinmann, P., 2003a. Geometrically nonlinear anisotropic inelasticity based on fictitious configurations: Application to the coupling of continuum damage and multiplicative elasto-plasticity. Int. J. Numer. Meth. Eng. 56, 2233–2266.
Menzel, A., Steinmann, P., 2003b. On the spatial formulation of anisotropic multiplicative elasto-plasticity. Comput. Methods Appl. Mech. Eng. 192, 3431–3470.
Menzel, A., Steinmann, P., 2003c. A view on anisotropic finite hyper-elasticity. Eur. J. Mech. A/Solids 22, 71–87.
Miehe, C., 1995. A theory of large-strain isotropic thermoplasticity based on metric transformation tensors. Arch. Appl. Mech. 66, 45–64.
Miehe, C., 1996a. Exponential map algorithm for stress updates in anisotropic multiplicative elastoplasticity for single crystals. Int. J. Numer. Meth. Eng. 39, 3367–3390.
Miehe, C., 1996b. Numerical computation of algorithmic (consistent) tangent moduli in large-strain computational inelasticity. Comput. Methods Appl. Mech. Eng. 134, 223–240.
Miehe, C., 1998. A constitutive frame of elastoplasticity at large strains based on the notion of a plastic metric. Int. J. Solids Struct. 35, 3859–3897.
Miehe, C., Stein, E., 1992. A canonical model of multiplicative elasto-plasticity: Formulation and aspects of the numerical implementation. Eur. J. Mech. A/Solids 11, 25–43, special issue.
Murakami, S., 1988. Mechanical modeling of material damage. ASME J. Appl. Mech. 55, 280–286.

Oden, J., 1972. Finite Elements of Nonlinear Continua. Advanced Engineering Series. McGraw-Hill, New York.

Oller, S., Botello, S., Miquel, J., Oñate, E., 1995. An anisotropic elastoplastic model based on an isotropic formulation. Eng. Comput. 12, 245–262.

Paulun, J., Ręcherski, R., 1992. On the relation for plastic spin. Arch. Appl. Mech. 62, 376–385.

Pérez-Foguet, A., Rodriguez-Ferran, A., Huerta, A., 2000a. Numerical differentiation for local and global tangent operators in computational plasticity. Comput. Methods Appl. Mech. Eng. 189, 277–296.

Pérez-Foguet, A., Rodriguez-Ferran, A., Huerta, A., 2000b. Numerical differentiation for non-trivial consistent tangent matrices: An application to the MRS–Lade model. Int. J. Numer. Meth. Eng. 48, 159–184.

Rappaz, M., Bellet, M., Deville, M., 2003. Numerical Modeling in Material Science and Engineering. In: Springer Series in Computational Mathematics, vol. 32. Springer, Berlin.

Sidoroff, F., 1981. Description of anisotropic damage application to elasticity. In: Hult, J., Lemaitre, J. (Eds.), Physical Non-Linearities in Structural Analysis. In: IUTAM Symposium Senlis/France, 27–30.05.1980. Springer, Berlin, pp. 237–244.

Simo, J., 1998. Numerical analysis and simulation of plasticity. In: Ciarlet, P., Lions, J. (Eds.), Numerical Methods for Solids (Part 3). In: Handbook of Numerical Analysis, vol. VI. North-Holland, Amsterdam, pp. 183–499.

Simo, J., Armero, F., 1992. Geometrically non-linear enhanced strain mixed methods and the method of incompatible modes. Int. J. Numer. Meth. Eng. 33, 1413–1449.

Steinmann, P., Carol, I., 1998. A framework for geometrically nonlinear continuum damage mechanics. Int. J. Eng. Sci. 36, 1793–1814.

Steinmann, P., Miehe, C., Stein, E., 1994. Comparison of different finite deformation inelastic damage models within multiplicative elastoplasticity for ductile materials. Comput. Mech. 13, 458–474.

Steinmann, P., Miehe, C., Stein, E., 1996. Fast transient dynamic plane stress analysis of orthotropic Hill-type solids at finite elastoplastic strains. Int. J. Solids Struct. 33, 1543–1562.

Svendsen, B., 1998. A thermodynamic formulation of finite-deformation elastoplasticity with hardening based on the concept of material isomorphism. Int. J. Plasticity 14, 473–488.

Svendsen, B., Arndt, S., Klingbeil, D., Sievert, R., 1998. Hyperelastic models for elastoplasticity with non-linear isotropic and kinematic hardening at large deformation. Int. J. Solids Struct. 35, 3363–3389.

Tsakmakis, C., 2004. Description of plastic anisotropy effects at large deformations. Part I: Restrictions imposed by the second law and the postulate of Il'iushin. Int. J. Plasticity 20, 167–198.

Wallin, M., Ristinmaa, M., Ottosen, N., 2003. Kinematic hardening in large strain plasticity. Eur. J. Mech. A/Solids 22, 341–356.

Weber, G., Anand, L., 1990. Finite deformation constitutive equations and a time integration procedure for isotropic, hyperelastic-viscoplastic solids. Comput. Methods Appl. Mech. Eng. 79, 173–202.